Oncogene (2010) 29, 2228–2237

www.nature.com/onc

ORIGINAL ARTICLE

Accelerated hepatocellular carcinoma development in mice expressing the *Pim-3* transgene selectively in the liver

Y Wu[1,2], YY Wang[2], Y Nakamoto[3], Y-Y Li[2,4], T Baba[2], S Kaneko[3], C Fujii[2,5] and N Mukaida[2]

[1]*Department of Hematology and Hematology research Laboratory, State Key Laboratory of Biotherapy and Cancer Center, West China Hospital, Sichuan University, Chengdu, Sichuan Province, PR China;* [2]*Division of Molecular Bioregulation, Cancer Research Institute, Kanazawa University, 13-1 Takara-machi, Kanazawa, Japan;* [3]*Department of Disease Control and Homeostasis, Graduate School of Medical Sciences, Kanazawa University, 13-1 Takara-machi, Kanazawa, Japan and* [4]*Researcher Center, Fudan University Cancer Hospital, Shanghai, PR China*

Pim-3, a proto-oncogene with serine/threonine kinase activity, was enhanced in hepatocellular carcinoma (HCC) tissues. To address the roles of Pim-3 in HCC development, we prepared transgenic mice that express human Pim-3 selectively in liver. The mice were born at a Mendelian ratio, were fertile and did not exhibit any apparent pathological changes in the liver until 1 year after birth. Pim-3-transgenic mouse-derived hepatocytes exhibited accelerated cell cycle progression. The administration of a potent hepatocarcinogen, diethylnitrosamine (DEN), induced accelerated proliferation of liver cells in Pim-3 transgenic mice in the early phase, compared with that observed for wild-type mice. Treatment with DEN induced lipid droplet accumulation with increased proliferating cell numbers 6 months after the treatment. Eventually, wild-type mice developed HCC with a frequency of 40% until 10 month after the treatment. Lipid accumulation was accelerated in Pim-3 transgenic mice with higher proliferating cell numbers, compared with that observed for wild-type mice. Pim-3 transgenic mice developed HCC with a higher incidence (80%) and a heavier burden, together with enhanced intratumoral CD31-positive vascular areas, compared with that observed for wild-type mice. These observations indicate that Pim-3 alone cannot cause, but can accelerate HCC development when induced by a hepatocarcinogen, such as DEN.
Oncogene (2010) **29,** 2228–2237; doi:10.1038/onc.2009.504; published online 18 January 2010

Keywords: serine/threonine kinase; apoptosis; cell cycle; Bad

Correspondence: Dr N Mukaida, Division of Molecular Bioregulation, Cancer Research Institute, Kanazawa University, 13-1 Takara-machi, Kanazawa, Ishikawa 920-0934, Japan.
E-mail: naofumim@kenroku.kanazawa-u.ac.jp
[5]Present address, Department of Integrative Physiology, School of Medicine, Shinshu University, 3-1-1 Asahi, Matsumoto 390-8621, Japan.
Received 13 May 2009; revised 25 October 2009; accepted 7 December 2009; published online 18 January 2010

Introduction

There were over 667 000 new cases of hepatocellular carcinoma (HCC) worldwide in 2005. The 5-year survival rate of individuals with hepatic malignancy is only 8.9% despite aggressive conventional therapy, making hepatic malignancy the second most lethal cancer among human malignancies (Farazi and DePinho, 2006; Umemura *et al.*, 2009). Hepatocellular carcinoma usually arises in conditions that can cause liver cirrhosis, such as chronic hepatitis B and C viral infection, chronic alcohol consumption and intake of food contaminated with aflatoxin-B_1 (Zheng *et al.*, 2007). These conditions generally provoke continuous rounds of hepatocyte damage in the setting of chronic hepatitis or liver cirrhosis, and eventually activate resident or inflammatory non-parenchymal cells to produce growth factors and cytokines (Otani *et al.*, 2005). The produced factors can drive compensatory and aberrant proliferation of surviving hepatocytes and development of pre-malignant dysplastic nodules that form the nucleus of neoplastic lesions. Only recently has the molecular analysis of human HCC unraveled many genetic and epigenetic alterations that result in the deregulation of key proto-oncogenes and tumor-suppressor genes, including TP53, β-catenin, ErbB receptors family members, *met* and its ligand, hepatocyte growth factor, p16, E-cadherin and cyclo-oxygenase 2 (Hosono *et al.*, 1993). However, roles of other proto-oncogenes and tumor suppressor genes in HCC development still remain elusive (Thorgeirsson and Grisham, 2002).

We previously identified *Pim-3*, a proto-oncogene with serine/threonine kinase activity, as the gene selectively expressed in pre-malignant and malignant lesions of the mouse HCC model in transgenic mice expressing hepatitis B virus surface antigen (Fujii *et al.*, 2005). *Pim-3* was originally identified as a depolarization-induced gene, *KID-1*, in PC12 cells, a rat pheochromocytoma cell line (Feldman *et al.*, 1998). Subsequently, Deneen *et al.* (2003) demonstrated that *Pim-3* gene transcription was enhanced in the EWS/ETS-induced malignant transformation of NIH 3T3 cells, suggesting the involvement of Pim-3 in tumorigenesis. Consistently, we observed that Pim-3 expression was enhanced in

carcinomas but not in normal tissues of human endoderm-derived organs, including the liver (Fujii *et al.*, 2005), pancreas (Li *et al.*, 2006), colon (Popivanova *et al.*, 2007) and stomach (Zheng *et al.*, 2008). Moreover, Pim-3 can inactivate a pro-apoptotic molecule, Bad, and maintain the expression of an anti-apoptotic molecule, Bcl-X_L, and prevent apoptosis of human pancreatic cancer and colon cancer cells (Li *et al.*, 2006). Similarly, the ablation of endogenous Pim-3 by short interfering RNA reduced the cell growth of human HCC cell lines by inducing their apoptosis (Fujii *et al.*, 2005).

These observations prompted us to investigate the effects of liver-specific Pim-3 overexpression on HCC development. Although we could not observe spontaneous HCC development in liver-specific Pim-3 transgenic mice, these mice developed HCC with a higher incidence and a heavier hepatocarcinoma burden, when a potent hepatocarcinogen, diethylnitrosamine (DEN), was administered during the suckling period. These results suggest that Pim-3 can accelerate but is not likely the primary inducer of HCC development.

Results

Characterization of transgenic mice overexpressing Pim-3 under the control of the albumin promoter

Pim-3 transgenic mice were born at a Mendelian ratio, were fertile and did not show any apparent abnormalities in the liver until 1 year after birth (data not shown). We first examined the expression pattern of Pim-3 in Pim-3 transgenic mice. Mouse *Pim-3* messenger RNA (mRNA) was detected in liver at a similar extent in both wild-type (WT) and Pim-3 transgenic mice, whereas human *Pim-3* mRNA was exclusively detected in Pim-3 transgenic mice (Figure 1b). Consistently, Pim-3 protein was detected abundantly in liver of Pim-3 transgenic mice but not WT mice (Figure 1b). Pim-3 protein was also detected in the heart and kidney of Pim-3 transgenic mice, but not of WT mice (Figure 1c). As anti-Pim-3 recognizes both human and mouse Pim-3 to a similar degree, we further examined the mRNA of human and mouse Pim-3 in the liver, heart and kidney. Human *Pim-3* mRNA was detected in the liver of Pim-3 transgenic mice, but not in other organs (Figure 1d). These observations would indicate that Pim-3 transgenic mice express human Pim-3 abundantly and selectively in liver.

Enhanced hepatocyte proliferation by Pim-3 overexpression

As Pim-3 can phosphorylate a pro-apoptotic molecule, Bad, at the Ser^{112} residue but not at the Ser^{136} residue, we first examined the phosphorylation states of Bad, to prove the functionality of the *Pim-3* gene, selectively overexpressed in liver. Bad was constitutively phosphorylated at Ser^{112} in hepatocytes from Pim-3 transgenic but not WT mice (Figure 2a). However, the level of phospho-Ser^{136}–Bad was not enhanced in Pim-3 transgenic mice. These observations would indicate that overexpressed Pim-3 was functional in terms of its capacity to phosphorylate Bad, its substrate. The levels of cyclin D1 and proliferating cell nuclear antigen (PCNA) in hepatocytes were increased in Pim-3 transgenic mice, compared with that observed for WT mice (Figure 2b). Moreover, cell cycle analysis of isolated heptocytes revealed that the proportion of the cells in subG1 phase, which represent apoptotic cells, was marginally but not significantly decreased in Pim-3 transgenic mice. However, the proportion of the cells in G2/M phase was significantly increased in Pim-3 transgenic mice compared with that observed for WT mice (Figure 2c). To exclude the possibility that

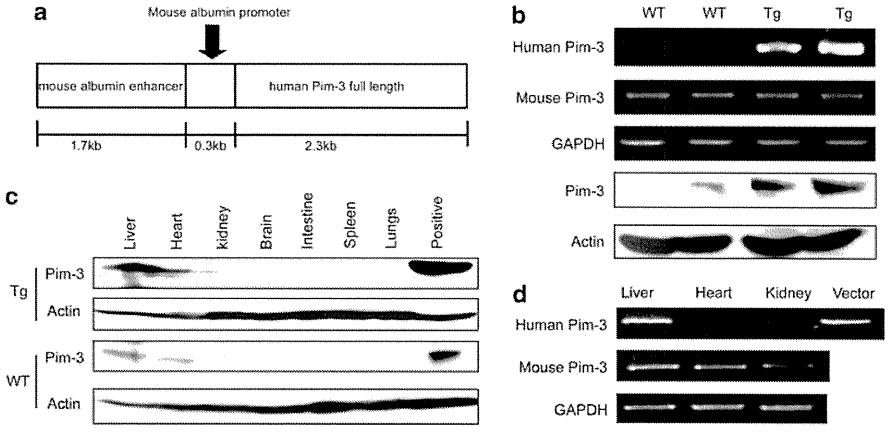

Figure 1 Expression of Pim-3 in alb-Pim-3 transgenic mice. (**a**) The schematic representation of the gene used for preparation of Pim-3 transgenic mice. (**b**) Expression of human (transgenic) and mouse (endogenous) *Pim-3* mRNA and protein levels in liver. The upper three lines are assessed by RT–PCR, whereas the lower two lines are assessed by immunoblotting. Representative results from five independent animals are shown here. (**c**) Immunoblotting analysis of Pim-3 protein expression in the liver, heart, kidney, brain, intestine, spleen and lungs of Pim-3 transgenic mice. The human embryonic kidney (HEK293) cells transfected with human Pim-3 complementary DNA (cDNA) were used as a positive control. Representative results from five independent animals are shown here. (**d**) Endogenous mouse *Pim-3* mRNA expression in the liver, heart and kidney of Pim-3 transgenic mice were determined by RT–PCR. Representative results from five independent animals are shown here.

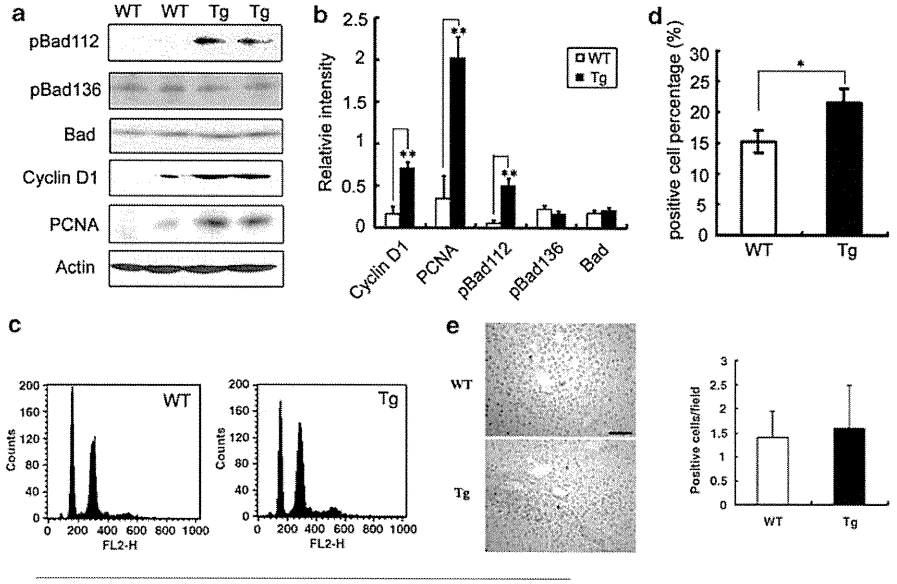

	subG1	G0/G1	S	G2/M	polyploidy
WT	0.87±0.29	40.52±1.12	2.51±0.69	50.40±1.63	5.7±0.54
Tg	0.38±0.12	31.68±0.83*	1.19±0.27	57.19±0.77*	9.55±0.51*

Figure 2 The effects of Pim-3 overexpression on hepatocyte functions. Hepatocytes were obtained from 3-week-old wild-type (WT) and Pim-3 transgenic (Tg) mice and used for the following analyses. (**a** and **b**) Protein was extracted from purified hepatocytes from WT and Tg mice, and was subjected to immunoblotting using anti-phospho-Ser^{112}-Bad, anti-phospho-Ser^{136}-Bad, anti-Bad, anti-cyclin D1 and anti-PCNA (proliferating cell nuclear antigen) antibodies as described in Materials and methods section. Representative results from four independent experiments are shown in (**a**). The intensity of each band was determined using National Institutes of Health (NIH) Image Analysis software version 1.62 (NIH, Bethesda, MD, USA), and its ratios to β-actin were calculated and are shown in (**b**) ($n=4$). Open boxes, WT mice; closed boxes, Pim-3 Tg mice. $^{**}P<0.01$. (**c**) DNA contents were determined for hepatocytes from WT and Pim-3 Tg mice as described in Materials and methods section. Representative results from five independent experiments are shown here. After the proportion of each fraction was determined, mean and 1 s.d. were calculated and are shown in the Table (inlet; $n=5$). $^{\#}P<0.05$; $^{*}P<0.01$. (**d**) The proportion of cyclin B1-positive cells was determined on liver tissues obtained from 3-week-old Pim-3 trangenic and WT mice as described in Materials and methods section. Mean and s.e.m. values were calculated ($n=6$) and are shown here. (**e**) The terminal transferase dUTP nick end labeling (TUNEL) assay was conducted as described in Materials and methods section. Representative results from five individual animals are shown in the left panel. Positive cells were determined in five randomly chosen fields (× 400) from each animal by an examiner without any knowledge of experimental procedures. Mean ± s.d. values are shown in the right panel ($n=5$).

isolation of hepatocytes from liver gave rise to artificially high proportion of cells in G2/M phase, we also enumerated the proportion of cells in G2/M phase by immunostaining liver tissues with anti-cyclin B1 antibodies. The proportion of cyclin B1-positive cells were significantly higher in Pim-3 transgenic mice than in WT mice (Figure 2d). Moreover, TUNEL (terminal transferase dUTP nick end labeling) staining failed to detect any significant differences in the numbers of apoptotic hepatocytes between untreated WT and Pim-3 transgenic mice (Figure 2e). These observations suggest that Pim-3 overexpressed in liver can accelerate the cell cycle progression of hepatocytes.

Enhanced liver damage in Pim-3 transgenic mice

We then treated Pim-3 transgenic and WT mice with DEN, a potent hepatocarcinogen. Both Pim-3 transgenic and WT mice survived exposure to DEN. Serum alanine amino transferase levels, a marker of liver injury, increased with maximal levels less than 1 000 IU/l, and were significantly but not markedly higher in Pim-3 transgenic mice than in WT mice (Figure 3a). These observations suggest that DEN-induced acute liver injury was mild. This may account for comparable levels of apoptosis in liver after DEN treatment until 72 h after the injection (Figures 3b and c). In contrast, PNCA and cyclin D1 levels were higher, at 72 h after the injection in Pim-3 transgenic mice, than those observed for WT mice (Figures 3d and e). Moreover, proliferating cells were progressively increased in the centrilobular region of Pim-3 transgenic mice and to a lesser degree in WT mice (Figures 3f and g). The crucial involvement of tumor necrosis factor (TNF)-α in hepatocyte proliferation (Yamada *et al*., 1997) prompted us to determine intrahepatic expression of TNF-α mRNA levels. The TNF-α mRNA levels were increased significantly at 48 h after DEN treatment (Figure 3h). These observations

indicate that the DEN challenge enhanced liver damage in Pim-3 transgenic mice, compared with that observed for WT mice, despite increased hepatocyte proliferation.

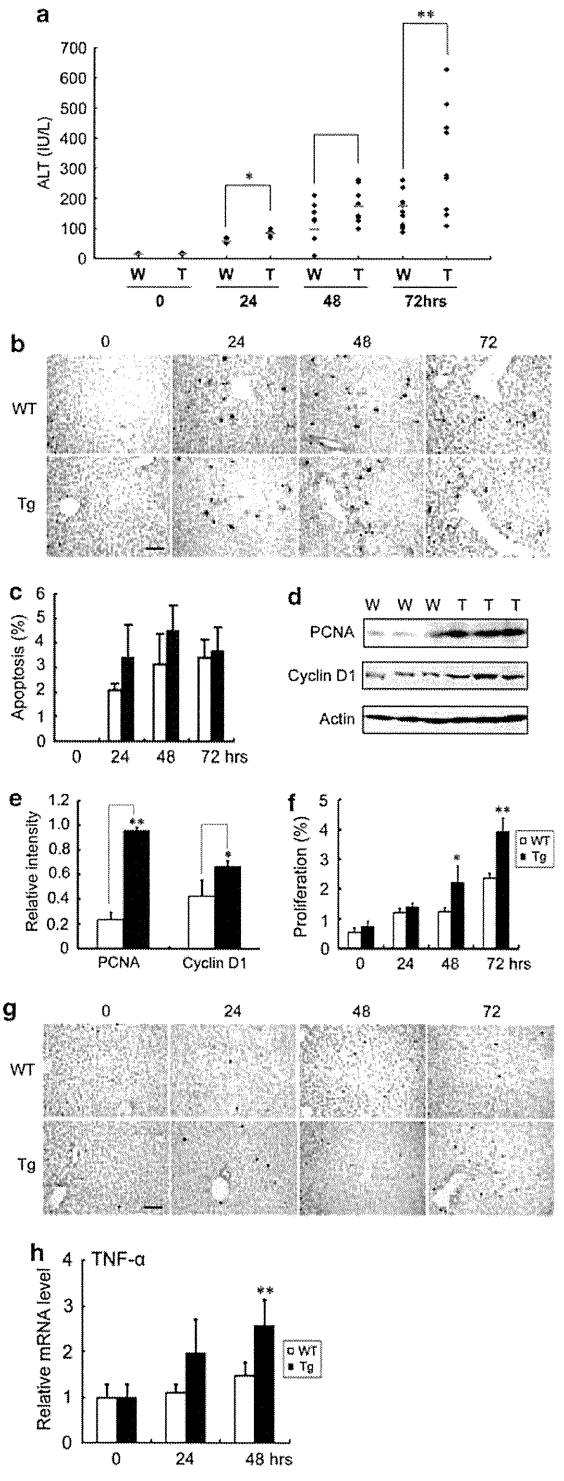

Enhanced hepatocarcinogenesis in Pim-3 transgenic mice

We next examined the changes in liver in the later phase of DEN treatment. As lipid droplet accumulation precedes the onset of DEN-induced HCC development (Wang *et al.*, 2009), we examined the lipid droplet accumulation in liver after DEN treatment. Lipid droplet accumulation was more evident in Pim-3 transgenic mice than in WT mice, until 6 months after DEN treatment (Figure 4a). The PCNA-positive proliferating cell numbers were progressively increased in Pim-3 transgenic mice and to a lesser degree in WT mice (Figures 4b and c). Tumor necrosis factor-α was potentially involved in hepatocarcinogenesis (Roberts and Kimber, 1999; Schwabe and Brenner, 2006). Moreover, its expression was enhanced to a greater extent in Pim-3 transgenic mice than that observed for WT mice promptly after treatment with a high-dose of DEN (Figure 3h). Hence, we investigated *TNF-α* mRNA expression in the course of hepatocarcinogenesis together with other pro-inflammatory cytokines, such as interleukin-1. Indeed, *TNF-α* mRNA expression was enhanced in Pim-3 transgenic and WT mice after DEN treatment, but the increase was more evident in Pim-3 transgenic mice (Figure 4f). A similar tendency was observed for interleukin-1β but not for interleukin-1α (Figures 4d and e). Dysplastic cells were observed and lobules were distorted in livers of Pim-3 transgenic mice, but not of WT mice, 6 months after DEN treatment (Figure 5a). At 10 months after the injection, nodules consisting of highly dysplastic malignant cells were observed in liver of Pim-3 transgenic mice and to a lesser extent in WT mice (Figure 5a). Macroscopically,

Figure 3 The effects of overexpressed Pim-3 on apoptosis and cell proliferation after diethylnitrosamine (DEN) treatment. (**a**) Serum alanine amino transferase (ALT) levels were determined as described in Materials and methods section. Each symbol indicates serum ALT level of each animal and the bars represent the median of each group. $*P<0.05$; $**P<0.01$ vs wild-type (WT) mice. (**b** and **c**) Liver tissues were obtained from WT or transgenic (Tg) mice at the indicated time intervals and immunostained with anti-cleaved caspase 3 antibody. Representative results from five independent animals are shown in (**b**) with an original magnification ×400. Proportion of cleaved caspase 3-positive apoptotic cells were determined as described in Materials and methods section. Mean ± s.d. values are shown in (**c**) ($n=5$). Open boxes, WT mice; closed boxes, Pim-3 transgenic mice. (**d** and **e**) Cell lysates were obtained from liver of WT (W) and Pim-3 transgenic mice (T) at 72 h after DEN treatment and subjected to immunoblotting using anti-PCNA (proliferating cell nuclear antigen) or anti-cyclin D1 antibodies. Representative results from three independent experiments are shown in (**d**). The intensity of each band was determined and its ratio to β-actin was calculated. Mean ± s.d. values are shown in (**e**) ($n=5$). Open boxes, WT mice; closed boxes, Pim-3 transgenic mice. $*P<0.05$; $**P<0.01$ vs WT mice. (**f** and **g**) Liver tissues were obtained from WT or Tg mice at the indicated time intervals and immunostained with anti-PCNA antibody. Representative results from five independent animals are shown in (**g**) with an original magnification ×400. PCNA-positive proliferating cell numbers were determined as described in Materials and methods section. Mean ± s.d. values are shown in (**f**) ($n=5$). $*P<0.05$; $**P<0.01$ vs WT mice. (**h**) Intrahepatic tumor necrosis factor-α (*TNF-α*) mRNA levels were determined as described in Materials and methods section. $**P<0.01$ vs WT mice ($n=5$).

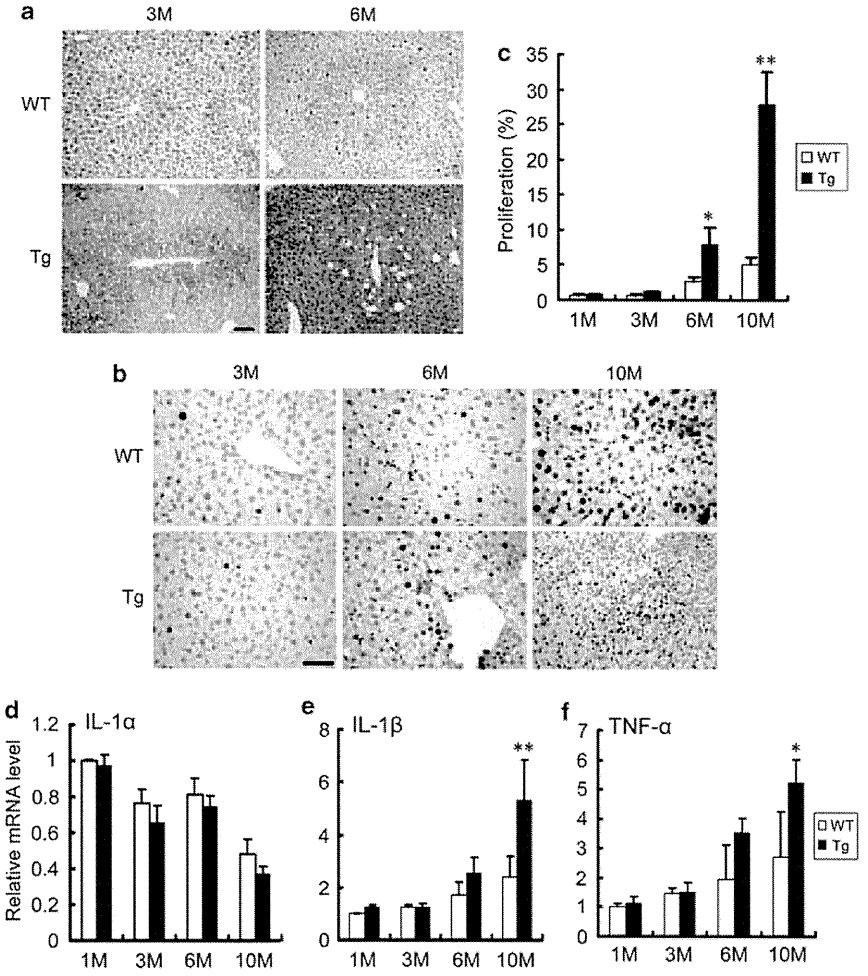

Figure 4 The effects of Pim-3 overexpression in liver pathology in the later phase after diethylnitrosamine (DEN) treatment. (**a**) The liver was obtained from wilt-type (WT) or Pim-3 transgenic mice (Tg) at the indicated time intervals and was subjected to staining with oil red solution as described in Materials and methods section. Representative results from five independent animals are shown with an original magnification ×200. (**b** and **c**) The livers were obtained from WT or Pim-3 Tg mice at the indicated time intervals and were subjected to immunostaining with anti-PCNA (proliferating cell nuclear antigen) antibody as described in Materials and methods section. Representative results from five independent animals are shown in (**b**) with an original magnification ×400. PCNA-positive cell numbers were determined as described in Materials and methods section. Mean ± s.d. values are shown in (**c**) ($n=5$). Open boxes, WT mice; closed boxes, Pim-3 Tg mice. $^*P<0.05$; $^{**}P<0.01$ vs WT mice.(**d**, **e** and **f**) Total RNA was extracted from the liver of WT or Pim-3 Tg mice at the indicated time intervals after DEN treatment and were subjected to a semi-quantitative RT–PCR analysis for the detection of mRNA for interleukin (IL)-1α (**d**), IL-1β (**e**), and tumor necrosis factor (TNF)-α (**f**). The ratio of each cytokine was calculated as described in Materials and methods section. Each value represents mean ± s.d. value ($n=5$). Open boxes, WT mice; closed boxes, Pim-3 Tg mice. $^*P<0.05$; $^{**}P<0.01$ vs WT mice.

approximately half of male WT mice developed HCC nodules at 10 months after DEN injection (Figures 5b–d), consistent with the previous report (Yang *et al.*, 2006). In contrast, most Pim-3 transgenic mice developed HCC nodules by 10 months after DEN treatment, with higher relative liver weight and larger numbers of HCC nodules than WT mice (Figures 5b–e). The enhanced hepatocarcinogenesis in Pim-3 transgenic mice may mirror the fact that neovascularization, an essential process for hepatocarcinogenesis, was augmented in Pim-3 transgenic mice compared with that observed for WT mice, as demonstrated by increases in CD31-positive areas in the liver (Figures 5f and g).

Discussion

We previously observed that Pim-3 was expressed selectively in pre-malignant and malignant lesions of the mouse HCC model in transgenic mice expressing hepatitis B virus surface antigen (Fujii *et al.*, 2005). Moreover, Pim-3 protein was detected in a substantial proportion of HCC cells and precancerous lesions in human liver samples, but not normal human liver. Furthermore, Pim-3 protein was also detected in regenerating bile ductules that are assumed to be the proliferation of hepatic stem cells after chronic injury. These observations suggested potential roles of aberrantly expressed Pim-3 in hepatocarcinogenesis. To

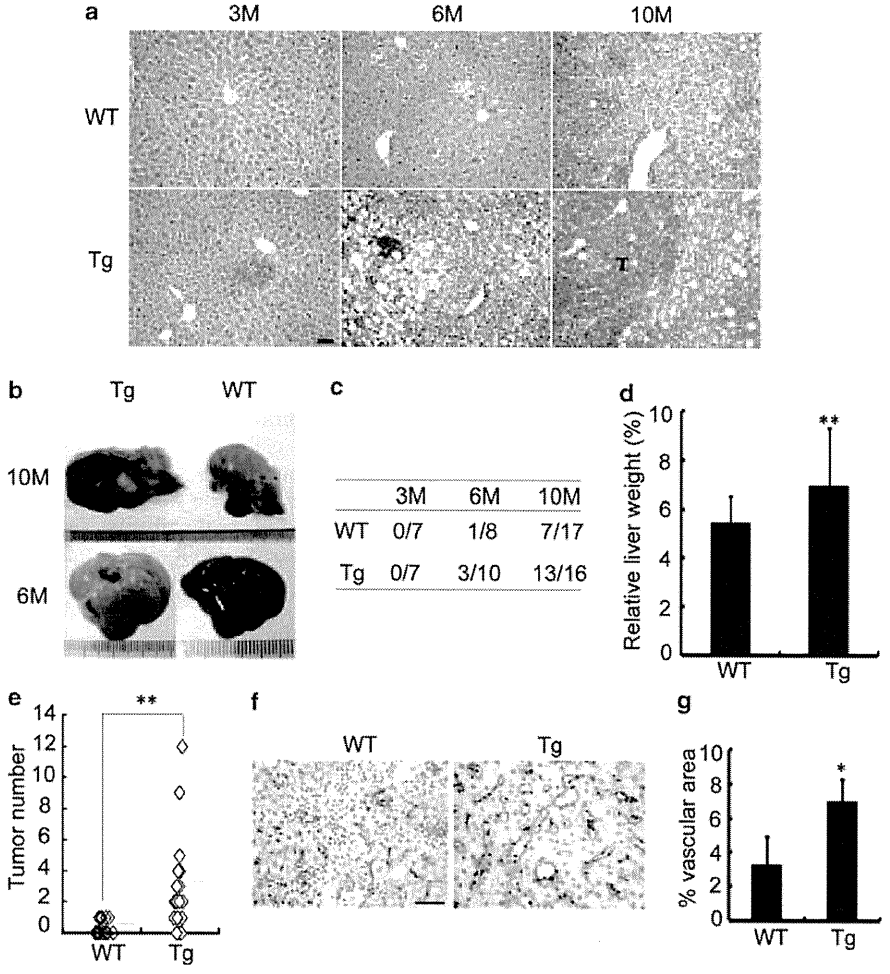

Figure 5 Enhanced hepatocarcinogenesis in Pim-3 transgenic (Tg) mice. (**a**) The liver tissues were obtained from wild-type (WT) or Pim-3 Tg mice at the indicated time intervals after DEN treatment and subjected to hematoxylin and eosin (HE) staining. Representative results from five individual animals are shown here with an original magnification ×200. (**b**) Macroscopic appearance of liver at 10 and 6 months after DEN treatment. Representative results from eight animals are shown here. Left panels: Pim-3 Tg mice; right panels: WT mice. The arrow indicates a small tumor nodule. (**c**) Incidence of macroscopic tumor formation at the indicated time intervals after DEN treatment in WT and Pim-3 Tg mice. (**d**) Liver weight relative to whole body weight was determined for WT and Pim-3 Tg mice at 10 months after DEN treatment. Each value represents mean ± s.d. value ($n=5$). $^{**}P<0.01$ vs WT mice. (**e**) Numbers of tumors with a diameter of larger than 1 mm were determined in the livers of WT ($n=17$) or Pim-3 Tg mice ($n=16$) at 10 months after DEN treatment. Each symbol indicates the tumor numbers of each animal and the bars represent the median of each group. $^{**}P<0.01$ vs WT mice. (**f** and **g**) The liver tissues were obtained from WT or Pim-3 Tg mice at 10 months after DEN treatment and were subjected to immunostaining with anti-CD31 antibody. Representative results from five individual animals are shown in (**f**) with an original magnification ×400. CD31-positive vascular areas within tumors were determined as described in Materials and methods section. Mean and s.d. values were calculated and are shown in (**g**). $^{*}P<0.05$ vs WT mice.

address the roles of Pim-3, we generated transgenic mice that constitutively express human Pim-3 selectively in liver. Untreated hepatocytes derived from these transgenic mice exhibited enhanced cell proliferation compared with those obtained from WT mice. However, these transgenic mice did not develop HCC spontaneously. Hence, enhanced cell proliferation cannot *per se* result in carcinogenesis in liver.

Kinase activation generally requires a posttranslational modification, particularly, phosphorylation in its regulatory domain. However, another member of the Pim kinase family, Pim-1, is constitutively active without any further alteration in its conformation because it lacks any regulatory domain (Qian *et al.*, 2005). Similarly, Pim-3 lacks any regulatory domain (Fujii *et al.*, 2005) and *Pim-3* complementary DNA (cDNA) alone induced phosphorylation of its target protein, Bad, at Ser^{112} when it was transfected into human pancreatic cancer cell lines (Li *et al.*, 2006). Consistently, Pim-3 transgenic mice exhibited enhanced phosphorylation of Bad at Ser^{112} in the liver. The proapoptotic activity of Bad is regulated by its phosphorylation at

Ser^{112} or Ser^{136} (She *et al.*, 2005). Unphosphorylated Bad binds and eventually inactivates anti-apoptotic family members, primarily Bcl-X_L and even Bcl-2 (Yang *et al.*, 1995; Zha *et al.*, 1996). As phosphorylation of Bad at Ser^{112} or Ser^{136} can result in the liberation of Bcl-X_L and Bcl-2, which can prevent apoptosis (Chen *et al.*, 2005), phosphorylated Bad represents its inactive form. However, both WT and Pim-3 transgenic mice developed apoptosis in liver to a similar extent when they were treated with a potent hepatocarcinogen, DEN. These observations suggest that phosphorylated Bad is not sufficient to prevent apoptosis induced by potent hepato-cytotoxic drugs such as DEN.

Pim-3 transgenic mice developed HCC with a higher incidence and a heavier burden than WT mice when both were treated similarly with DEN. Hepatocytes, particularly those in the centrilobular region, metabolized DEN into an alkylating agent that, in turn, can induce DNA damage and mutations in hepatocytes (Verna *et al.*, 1996). Simultaneously, DEN metabolites can generate reactive oxygen species (ROS) (Kamata *et al.*, 2005; Schwabe and Brenner, 2006). When treated with DEN, mice with liver-specific deletion of an essential kinase for NF-κB activation, IKKβ, generated increased levels of ROS in hepatocytes, together with enhanced hepatocyte death and augmented compensatory hepatocyte proliferation. The net result was exaggerated HCC development with a high cell proliferation rate as evidenced by increased PCNA- and cyclin D1-positive cell numbers in liver (Maeda *et al.*, 2005). Similarly, DEN treatment augmented hepatocyte proliferation but not apoptosis in Pim-3 transgenic mice compared with that observed in WT mice, as evidenced by increased PCNA- and cyclin D1-positive cell numbers in liver. These data may account for accelerated hepatocarcinogenesis in Pim-3 transgenic mice. However, several lines of evidence indicate the potential involvement of other Pim kinases, Pim-1 and Pim-2, in NF-κB activation (Hammerman *et al.*, 2004; Zemskova *et al.*, 2008). Thus, it still remains to be investigated whether the *Pim-3* transgene can induce ROS generation in a similar manner as the IKKβ deletion.

Liver injury causes liver regeneration primarily through hepatocyte division but if hepatocyte division is impaired, liver repair requires the recruitment of hepatic oval cells (Ma *et al.*, 2006). Oval cells mainly express α-fetoprotein but not albumin, and can proliferate and differentiate into both hepatocytes and bile duct cells. Several independent groups claimed that HCC cells can arise from oval cells (Braun *et al.*, 1989). Mice deficient in the *IKKβ* gene in liver developed HCC with an incidence higher than WT mice (Maeda *et al.*, 2005). In this mouse, the *IKKβ* gene was deleted by using cre recombinase expressed under the control of an albumin promoter/enhancer and therefore, the gene was deleted selectively in albumin-expressing hepatocytes but not in oval cells. As we used the same promoter/enhancer to prepare transgenic mice, it is likely that the *Pim-3* transgene was expressed selectively in hepatocytes but not in oval cells. Thus, the *Pim-3* transgene mainly acted on hepatocytes to promote carcinogenesis, although its effects on oval cell proliferation cannot completely be excluded.

Accumulating evidence indicates that Pim-1, a member of the Pim kinase family, can progress cell cycle by phosphorylating several cell cycle regulators and altering their activities. Pim-1 can phosphorylate the phosphatase, Cdc25A, thereby increasing its phosphatase activity (Mochizuki *et al.*, 1999). Moreover, Pim-1 can phosphorylate G1-specific inhibitor p21 (Waf), a cyclin-dependent kinase inhibitor, and induce its cytoplasmic localization (Wang *et al.*, 2002). Furthermore, Pim-1 can phosphorylate the kinase Cdc25C-associated kinase (C-TAK)-1 and decrease its kinase activity (Bachmann *et al.*, 2004), whereas Pim-1 can phosphorylate and activate the G2/M-specific phosphatase Cdc25C. Alteration of the activities of these molecules can result in cell cycle progression, particularly during the G2/M phase. Pim-3 and Pim-1, but not Pim-2, bind to a consensus peptide substrate (AKRRRHPSGPPTA) with a strikingly high affinity, having K_d value in the range of 40–60 nM (Bullock *et al.*, 2005). Thus, it is likely that Pim-3 can phosphorylate these cell cycle regulators similarly as Pim-1. Supporting this idea, recombinant Pim-3 protein can phosphorylate p21/Waf *in vitro* (Morishita *et al.*, 2008). This may account for the observations that cell cycle progression was accelerated in Pim-3 transgenic mouse-derived hepatocytes compared with WT mice, as evidenced by increased proportion of the cells in G2/M phase and reciprocally decreased proportion of the cells in G0/G1 phase.

The hepatocarcinogen, DEN, induced TNF-α production consistently with the previous report (Sakurai *et al.*, 2006) and the production was further augmented by Pim-3 overexpression in liver. The crucial involvement of TNF-α in hepatocyte proliferation was proposed by the observation that liver regeneration after partial hepatectomy was impaired in mice deficient in *TNF* receptor gene (Yamada *et al.*, 1997). Moreover, accumulating evidence indicates the potential contribution of TNF-α to hepatocarcinogenesis (Roberts and Kimber, 1999; Schwabe and Brenner, 2006). Furthermore, TNF-α can promote angiogenesis, an essential process for tumorigenesis, by inducing the production of angiogenic factors, such as vascular endothelial growth factor and hepatocyte growth factor (Tamura *et al.*, 1993; Yoshida *et al.*, 1997). The production of TNF-α was regulated at several steps and the first one was at the transcription level, governed by transcription factors, such as NF-κB and Activator protein-1AP-1 (Manna *et al.*, 2000; Udalova and Kwiatkowski, 2001; Chung *et al.*, 2007). As Pim-1 can enhance NF-κB transcriptional activity (Zemskova *et al.*, 2008), Pim-3 might be able to similarly activate NF-κB, thereby inducing TNF-α expression.

It is most likely that our transgenic mice expressed a high level of the *Pim-3* transgene selectively in hepatocytes. A strong similarity of Pim-3 with another Pim kinase, Pim-1, suggests that Pim-3 can phosphorylate several cell cycle regulators and accelerate cell cycle progression as Pim-1 does. In support of this idea, we observed enhanced cell cycle progression in untreated

Pim-3 transgenic mouse-derived hepatocytes compared with that observed for WT mice. However, as evidenced by the absence of spontaneous HCC development in Pim-3 transgenic mice, accelerated hepatocyte proliferation alone cannot induce HCC. The hepatocarcinogen, DEN, can generate O^6-methlguanine and can frequently induce G-C-to-A-T transition mutations in hepatocytes (Nakatsuru *et al.*, 1993). The *Pim-3* transgene can enhance the proliferation of hepatocytes through G-C-to-A-T transition mutations, thereby accelerating HCC development. We previously observed that Pim-3 expression was detected in pre-malignant and malignant lesions but not in normal tissues of liver in humans and mice (Fujii *et al.*, 2005). Thus, Pim-3 may be a promoter but not an initiator of HCC development, and blocking of Pim-3 activity can delay and/or prevent HCC development.

Materials and methods

Preparation of Pim-3 transgenic mice

The mouse albumin enhancer/promoter region (Figure 1a) was a kind gift from Dr Palmiter (University of Washington, Seattle, WA, USA; Pinkert *et al.*, 1987). Full-length human *Pim-3* cDNA was subcloned 3 to this albumin enhancer/promoter gene. After being linearized by digestion with *Not*I, the gene was introduced into fertilized oocytes of C57BL/6 mice using a standard transgenic technique. Genomic DNA was isolated from the tail of the founder and offspring using Nucleospin tissue kit (Macherey Nagel, Düren, Germany) and genotyping was performed by PCR using a specific pair of primers, including a sense primer (5′-TTGAACTCATCGACC TGCAGGCAT-3′) flanking the upstream albumin promoter and an antisense primer (5′-GCCTTCTCGAAGCTCTCCTT GTCC-3′) inside the human *Pim-3* cDNA. Transgenic founder animals were mated with C57BL/6 mice (Charles River Japan, Yokohama, Japan). The male offspring with a heterozygous transgene were used as a transgenic group, whereas those without a transgene were used as a littermate control. All mice were kept under the specific pathogen-free conditions, and all animal experiments in this study complied with the Guidelines of the Care and Use of Laboratory Animals of Kanazawa University.

Hepatocyte isolation

Mouse hepatocytes were isolated by using a two-step perfusion method with some modifications. Briefly, under anesthetization with Avertin (2,2,2-tribromoethanol; Sigma-Aldrich, St Louis, MO, USA), a needle was inserted along the inferior vena cava and the liver was perfused sequentially with phosphate-buffered saline and collagenase-containing buffer at a rate of 5–10 ml/min. The liver was then dissected, suspended in ice-cold phosphate-buffered saline and filtered through a cell strainer with a pore size of 100 μm to remove connective tissue debris and cell clumps. After the cell suspensions were left on ice for 15 min, the resultant precipitates were collected, suspended in DMEM medium (Sigma-Aldrich) and centrifuged at 800 r.p.m. for 2 min. Cell suspensions were further centrifuged in 45% Percoll solution (Sigma-Aldrich) at 1000 r.p.m. for 10 min. The obtained cells were confirmed to consist of more than 95% hepatocytes on the basis of morphological criteria, with a viability of higher than 90% on trypan blue exclusion test. Purified hepatocytes were used for the following DNA content analysis and immunoblotting analysis.

Cell cycle analysis

The obtained hepatocytes were fixed with 70% ethanol at −20 °C. The fixed cells were incubated with 50 μg/ml propidium iodine (Molecular Probes, Eugene, OR, USA) and 1 μg/ml RNase A for 30 min at room temperature. The DNA content was then analyzed on a FACS Calibur system (BD Biosciences, Bedford, MA, USA). The distribution of cells in each cell-cycle phase was determined by cell ModFit LT software (BD Biosciences).

Protein extraction and western blotting

Hepatocytes or liver tissues were obtained and homogenized with RIPA buffer (Santa Cruz Biotechnology, Santa Cruz, CA, USA) containing proteinase inhibitor cocktail (Roche Diagnostics AG, Rotkreutz, Switzerland). After sonication for 1 min, homogenates were centrifuged at 15 000 *g* for 15 min at 4 °C to obtain the supernatants. After total protein concentrations were measured using a BCA kit (Pierce Biotechnology, Rockford, IL, USA), resultant supernatants were subjected to immunoblotting using anti-phospho-Ser^{112}-Bad, anti-phospho-Ser^{136}-Bad, anti-Bad, anti-Pim-3, anti-β actin (Sigma-Aldrich); anti-cyclin D1 (Cell Signaling Technology, Beverly, MA, USA) and anti-PCNA antibodies (BD Biosciences) as previously described (Li *et al.*, 2006).

Chemical-induced liver injury and subsequent hepatocarcinogenesis

Three-week old weaning mice were given a single intraperitoneal injection of DEN (Sigma-Aldrich), dissolved in physiological saline solution at a dose 10 mg/kg body weight as previously described (Yang *et al.*, 2006), to induce hepatocarcinogenesis. To induce acute liver injury, mice were given a dose of 100 mg/kg body weight. Serum alanine amino transferase levels were determined using a Fuji DRICHEM 55500V (Fuji Medical System, Tokyo, Japan) according to the manufacturer's instructions. Mice were killed at the indicated time intervals after the injection to conduct histopathological analysis.

RNA isolation and RT–PCR

Total RNAs were extracted from the organs using RNeasy mini kit (Qiagen, Hilden, Germany) according to the manufacturer's instructions and were further treated with RNase-free DNase (Promega, Madison, WI, USA) to deplete residual contaminated DNA. A total of 2 μg RNA was reverse-transcribed at 42 °C for 1 h in 20-μl reaction mixture containing Moloney murine leukemia virus reverse trancriptase (Toyobo, Osaka, Japan) and hexanucleotide random primer (Qiagen) to obtain cDNA as previously described (Wu *et al.*, 2008). Serially twofold diluted cDNA products were amplified for glyceraldehyde-3-phosphate dehydrogenase (GAPDH) using a specific set of primers (Table 1) using 25 cycles consisting of following reaction conditions: 94 °C for 30 s, 58 °C for 30 s and 72 °C for 1 min in a 25-μl of reaction mixture containing Taq polymerase (Takara Bio, Kyoto, Japan) to evaluate the quantity of the transcribed cDNA. Equal quantities of cDNA products were then amplified for the indicated genes using the specific sets of primers (Table 1) with 35 cycles consisting of following conditions: 94 °C for 30 s, 58 °C for 1 min and 72 °C for 1 min. The resultant PCR products were fractionated on 1.5% agarose gel and visualized by ethidium bromide staining under ultraviolet light trans-

Table 1 Sequences of the primers used for RT–PCR

Gene Name	*Forward*	*Reverse*	*Cycles*	*Length (bp)*
Mouse Pim-3	5′-GAGAGGGTCTCCCCAGAGT-3′	5′-TGGTGGCACGCTTAGGTTG-3′	35	660
Human Pim-3	5′-CGGAGGAGGGTCTCTCCAGAGTG-3′	5′-ACCCTGCGCCGGCGGAAAG-3′	35	535
Mouse TNF-α	5′-AGTTCTATGGCCCAGACCCT-3′	5′-CGGACTCCGCAAAGTCTAAG-3′	35	463
Mouse IL-1α	5′-CTCTAGAGCTCCATGCTACAGAC-3′	5′-TGGAATCCAGGGGAA ACACTG-3′	35	309
Mouse IL-1β	5′-ATGGCAACTGTTCCTGAACTCAAC T-3′	5′-CAGGACAGGTATAGATTCTTTCCTTTT-3′	35	377
GADPH	5′-ACCACAGTCCATGCCATCAC-3′	5′-TCCACCACCCTGTTGCTGTA-3′	25	431

Abbreviations: GADPH, glyceraldehydes-3-phosphate dehydrogenase; IL, interleukin; TNF, tumor necrosis factor.

illumination. The band intensities were measured using National Institutes of Health Image analysis software, version 1.62, and the ratios to GAPDH were calculated on the assumption that the ratios of untreated animals were set at 1.0.

Histopathological analysis

The liver tissue was fixed in 10% formalin buffered with phosphate-buffered saline (pH 7.2). and embedded in paraffin. Five-μm thick sections were stained with hematoxylin and eosin solution or subjected to the terminal transferase dUTP nick end labeling assay (MBL, Nagoya, Japan) according to the manufacturer's instructions. Immunohistochemical analysis was performed using anti-PNCA (BD Biosciences) or anti-cleaved caspase-3 antibodies (Cell Signaling Technology). A portion of the liver tissue was snap-frozen, dried at room temperature until the tissues firmly adhered to the slides, and was fixed in cold acetone for 10 min. The sections were blocked with serum-free Protein Block (Dako Cytomation, Glostrup, Denmark) and were incubated with rabbit anti-cyclin B1 antibodies (Santa Cruz Biotechnology). They were further incubated with Alexa Fluor 488-labeled donkey anti-rabbit IgG followed by counterstaining with 4-6-diamidino-2-phenylindole (Vector Laboratories, Burlingame, CA, USA) in dark. Immunoflurescence was visualized on a Laser Microscope 510 (Carl Zeiss, Hamburg, Germany) and cyclin B1-positive cell proportion was determined on 10 randomly chosen fields at $\times 200$ magnification. Another slides were used for staining with oil red (Sigma-Aldrich) and hematoxylin counterstaining, or immunohistochemical analysis using anti-CD31 antibodies (BD Pharmingen). The immune complexes were visualized by Envision+ System (Dako Cytomation), a catalyzed signal amplification system or the Elite ABC kit and DAB substrate kit (Vector Laboratories) according to the manufacturer's instructions. The positive cell numbers were enumerated on 10 randomly chosen visual fields at $\times 400$ magnification. The CD31-postive areas were determined as previously described (Wu *et al*., 2008). In brief, CD31-positive areas in the tumor tissue were defined as the intratumoral vascular areas. Areas of active neovascularization (hot spot) were found inside tumor foci by scanning the section at lower magnification and the pixel numbers of CD31-positive areas were then determined on five randomly chosen fields in hot spots of each animal at $\times 400$ magnification with the help of Photoshop version 7.0. The density of neovascularization was expressed as a percentage of the whole tumor area. All histopathological examinations were conducted by an examiner without any prior knowledge of the experimental procedures. All histopathological examinations were conducted blind, by an examiner without any prior knowledge of the experimental procedures.

Statistical analysis

All obtained data were calculated and expressed as mean ± s.d. The differences were analyzed statistically using one-way analysis of variance, followed by the Turkey–Kramer test. $P<0.05$ was considered statistically significant.

Conflict of interest

The authors declare no conflict of interest.

References

Bachmann M, Hennemann H, Xing PX, Hoffmann I, Moroy T. (2004). The oncogenic serine/threonine kinase Pim-1 phosphorylates and inhibits the activity of Cdc25C-associated kinase (C-TAK-1): a novel role for Pim-1 at the G2/M cell cycle checkpoint. *J Biol Chem* **279**: 48319–48328.

Braun L, Mikumo R, Fausto N. (1989). Production of hepatocellular carcinoma by oval cells: cell cycle expression of c-myc and p53 at different stages of oval cell transformation. *Cancer Res* **49**: 1554–1561.

Bullock AN, Debreczeni J, Amos AL, Knapp S, Turk BE. (2005). Structure and substrate specificity of the Pim-1 kinase. *J Biol Chem* **280**: 41675–41682.

Chen L, Willis SN, Wei A, Smith BJ, Fletcher JI, Hinds MG *et al*. (2005). Differential targeting of prosurvival Bcl-2 proteins by their BH3-only ligands allows complementary apoptotic function. *Mol Cell* **17**: 393–403.

Chung J, Koyama T, Ohsawa M, Shibamiya A, Hoshi A, Hirosawa S. (2007). 1,25(OH)(2)D(3) blocks TNF-induced monocytic tissue factor expression by inhibition of transcription factors AP-1 and NF-kappaB. *Lab Invest* **87**: 540–547.

Deneen B, Welford SM, Ho T, Hernandez F, Kurland I, Denny CT. (2003). PIM3 proto-oncogene kinase is a common transcriptional target of divergent EWS/ETS oncoproteins. *Mol Cell Biol* **23**: 3897–3908.

Farazi PA, DePinho RA. (2006). Hepatocellular carcinoma pathogenesis: from genes to environment. *Nat Rev Cancer* **6**: 674–687.

Feldman JD, Vician L, Crispino M, Tocco G, Marcheselli VL, Bazan NG *et al*. (1998). KID-1, a protein kinase induced by depolarization in brain. *J Biol Chem* **273**: 16535–16543.

Fujii C, Nakamoto Y, Lu P, Tsuneyama K, Popivanova BK, Kaneko S *et al*. (2005). Aberrant expression of serine/threonine kinase Pim-3 in hepatocellular carcinoma development and its role in the proliferation of human hepatoma cell lines. *Int J Cancer* **114**: 209–218.

Hammerman PS, Fox CJ, Cinalli RM, Xu A, Wagner JD, Lindsten T *et al*. (2004). Lymphocyte transformation by Pim-2 is dependent on nuclear κB activation. *Cancer Res* **64**: 8341–8348.

Hosono S, Chou MJ, Lee CS, Shih C. (1993). Infrequent mutation of *p53* gene in hepatitis B virus positive primary hepatocellular carcinomas. *Oncogene* **8**: 491–496.

Kamata H, Honda S, Maeda S, Chang L, Hirata H, Karin M. (2005). Reactive oxygen species promote TNFalpha-induced death and sustained JNK activation by inhibiting MAP kinase phosphatases. *Cell* **120**: 649–661.

Li YY, Popivanova BK, Nagai Y, Ishikura H, Fujii C, Mukaida N. (2006). Pim-3, a proto-oncogene with serine/threonine kinase activity, is aberrantly expressed in human pancreatic cancer and phosphorylates bad to block bad-mediated apoptosis in human pancreatic cancer cell lines. *Cancer Res* **66**: 6741–6747.

Ma W, Xia X, Stafford LJ, Yu C, Wang F, LeSage G *et al.* (2006). Expression of GCIP in transgenic mice decreases susceptibility to chemical hepatocarcinogenesis. *Oncogene* **25**: 4207–4216.

Maeda S, Kamata H, Luo JL, Leffert H, Karin M. (2005). IKKbeta couples hepatocyte death to cytokine-driven compensatory proliferation that promotes chemical hepatocarcinogenesis. *Cell* **121**: 977–990.

Manna SK, Mukhopadhyay A, Aggarwal BB. (2000). Leflunomide suppresses TNF-induced cellular responses: effects on NF-kappa B, activator protein-1, c-Jun N-terminal protein kinase, and apoptosis. *J Immunol* **165**: 5962–5969.

Mochizuki T, Kitanaka C, Noguchi K, Muramatsu T, Asai A, Kuchino Y. (1999). Physical and functional interactions between Pim-1 kinase and Cdc25A phosphatase. Implications for the Pim-1-mediated activation of the c-Myc signaling pathway. *J Biol Chem* **274**: 18659–18666.

Morishita D, Katayama R, Sekimizu K, Tsuruo T, Fujita N. (2008). Pim kinases promote cell cycle progression by phosphorylating and down-regulating p27Kip1 at the transcriptional and posttranscriptional levels. *Cancer Res* **68**: 5076–5085.

Nakatsuru Y, Matsukuma S, Nemoto N, Sugano H, Sekiguchi M, Ishikawa T. (1993). O^6-methylguanine-DNA methyltransgerase protects against nitrosamine-induced hepatocarcinogenesis. *Proc Natl Acad Sci USA* **90**: 6468–6472.

Otani K, Korenaga M, Beard MR, Li K, Qian T, Showalter LA *et al.* (2005). Hepatitis C virus core protein, cytochrome P450 2E1, and alcohol produce combined mitochondrial injury and cytotoxicity in hepatoma cells. *Gastroenterology* **128**: 96–107.

Pinkert CA, Ornitz DM, Brinster RL, Palmiter RD. (1987). An albumin enhancer located 10 kb upstream functions along with its promoter to direct efficient, liver-specific expression in transgenic mice. *Genes Dev* **1**: 268–276.

Popivanova BK, Li YY, Zheng H, Omura K, Fujii C, Tsuneyama K *et al.* (2007). Proto-oncogene, Pim-3 with serine/threonine kinase activity, is aberrantly expressed in human colon cancer cells and can prevent Bad-mediated apoptosis. *Cancer Sci* **98**: 321–328.

Qian KC, Wang L, Hickey ER, Studts J, Barringer K, Peng C *et al.* (2005). Structural basis of constitutive activity and a unique nucleotide binding mode of human Pim-1 kinase. *J Biol Chem* **280**: 6130–6137.

Roberts RA, Kimber I. (1999). Cytokines in genotoxic hepatocarcinogenesis. *Carcinogenesis* **20**: 1297–1401.

Sakurai T, Maeda S, Chang L, Karin M. (2006). Loss of hepatic NF-kappa B activity enhances chemical hepatocarcinogenesis through sustained c-Jun N-terminal kinase 1 activation. *Proc Natl Acad Sci USA* **103**: 10544–10551.

Schwabe RF, Brenner DA. (2006). Mechanisms of liver injury. I. TNF-alpha-induced liver injury: role of IKK, JNK, and ROS pathways. *Am J Physiol Gastrointest Liver Physiol* **290**: G583–G589.

She QB, Solit DB, Ye Q, O'Reilly KE, Lobo J, Rosen N. (2005). The BAD protein integrates survival signaling by EGFR/MAPK and PI3K/Akt kinase pathways in PTEN-deficient tumor cells. *Cancer Cell* **8**: 287–297.

Tamura M, Arakaki N, Tsuboushi H, Takada H, Daikuhara Y. (1993). Enhancement of human hepatocyte growth factor production by interleukin-1α and -1β and tumor necrosis factor-α by fibroblasts in culture. *J Biol Chem* **268**: 8140–8145.

Thorgeirsson SS, Grisham JW. (2002). Molecular pathogenesis of human hepatocellular carcinoma. *Nat Genet* **31**: 339–346.

Udalova IA, Kwiatkowski D. (2001). Interaction of AP-1 with a cluster of NF-kappa B binding elements in the human TNF promoter region. *Biochem Biophys Res Commun* **289**: 25–33.

Umemura T, Ichijo T, Yoshizawa K, Tanaka E, Kiyosawa K. (2009). Epidemiology of hepatocellular carcinoma in Japan. *J Gastroenterol* **44**(Suppl 19): 102–107.

Verna L, Whysner J, Williams GM. (1996). N-nitrosodiethylamine mechanistic data and risk assessment: bioactivation, DNA-adduct formation, mutagenicity, and tumor initiation. *Pharmacol Ther* **71**: 57–81.

Wang Y, Ausman LM, Geenberg AS, Russel RM, Wang X-D. (2009). Nonalcoholic steatohepatitis induced by a high-fat diet promotes diethylnitrosamine-initiated early hepatocarcinogenesis in rats. *In t J Cancer* **124**: 540–546.

Wang Z, Bhattacharya N, Mixter PF, Wei W, Sedivy J, Magnuson NS. (2002). Phosphorylation of the cell cycle inhibitor p21Cip1/WAF1 by Pim-1 kinase. *Biochim Biophys Acta* **1593**: 45–55.

Wu Y, Li YY, Matsushima K, Baba T, Mukaida N. (2008). CCL3–CCR5 axis regulates intratumoral accumulation of leukocytes and fibroblasts and promotes angiogenesis in murine lung metastasis process. *J Immunol* **181**: 6384–6393.

Yamada Y, Kirillova I, Peschon JJ, Fausto N. (1997). Initiation of liver growth by tumor necrosis factor: deficient liver regeneration in mice lacking type I tumor necrosis factor receptor. *Proc Natl Acad Sci USA* **94**: 1441–1446.

Yang E, Zha J, Jockel J, Boise LH, Thompson CB, Korsmeyer SJ. (1995). Bad, a heterodimeric partner for Bcl-XL and Bcl-2, displaces Bax and promotes cell death. *Cell* **80**: 285–291.

Yang X, Lu P, Fujii C, Nakamoto Y, Gao JL, Kaneko S *et al.* (2006). Essential contribution of a chemokine, CCL3, and its receptor, CCR1, to hepatocellular carcinoma progression. *Int J Cancer* **118**: 1869–1876.

Yoshida S, Ono M, Shono T, Izumi H, Ishibashi T, Suzuki H *et al.* (1997). Involvement of interleukin-8, vascular endothelial growth factor, and basic fibroblast growth factor in tumor necrosis factor α-dependent angiogenesis. *Mol Cell Biol* **17**: 4015–4023.

Zemskova M, Sahakian E, Bashkirova S, Lilly M. (2008). The PIM1 kinase is a critical component of a survival pathway activated by docetaxel and promotes survival of docetaxel-treated prostate cancer cells. *J Biol Chem* **283**: 20635–20644.

Zha J, Harada H, Yang E, Jockel J, Korsmeyer SJ. (1996). Serine phosphorylation of death agonist BAD in response to survival factor results in binding to 14-3-3 not BCL-X(L). *Cell* **87**: 619–628.

Zheng HC, Tsuneyama K, Takahashi H, Miwa S, Sugiyama T, Popivanova BK *et al.* (2008). Aberrant Pim-3 expression is involved in gastric adenoma-adenocarcinoma sequence and cancer progression. *J Cancer Res Clin Oncol* **134**: 481–488.

Zheng Y, Chen WL, Louie SG, Yen TS, Ou JH. (2007). Hepatitis B virus promotes hepatocarcinogenesis in transgenic mice. *Hepatology* **45**: 16–21.

Crucial Contribution of Thymic Sirpα^+ Conventional Dendritic Cells to Central Tolerance against Blood-Borne Antigens in a CCR2-Dependent Manner

Tomohisa Baba,* Yasunari Nakamoto,† and Naofumi Mukaida[1]*

Thymic dendritic cells (DCs) as well as thymic epithelial cells are presumed to be major sentinels in central tolerance by inducing the apoptosis of autoreactive T progenitor cells. The thymic DC population is composed of heterogeneous subsets including CD11c$^+$B220$^+$ plasmacytoid DCs, CD11c$^+$B220$^-$CD8α^+ signal regulatory protein α (Sirpα)$^-$ and CD11c$^+$B220$^-$CD8α^-Sirpα^+ conventional DCs (cDCs). However, the distinctive role of each DC subset remains undefined. We show herein that Sirpα^+ cDCs, a minor subpopulation, was disseminated in the thymic cortical area with some of them uniquely localized inside perivascular regions and nearby small vessels in the thymus. The Sirpα^+ but not Sirpα^- cDC subset can selectively capture blood-circulating Ags. Moreover, in CCR2-deficient mice, the thymic Sirpα^+ cDC subset, but not other thymic cell components, was moderately decreased especially in the perivascular regions. Concomitantly, these mice exhibited a modest impairment in intrathymic negative selection against blood-borne Ags, with the reduced capacity to uptake blood-borne Ags. Given their intrathymic cortical localization, CD11c$^+$B220$^-$CD8α^-Sirpα^+ cDCs can have a unique role in the development of central tolerance against circulating peripheral Ags, at least partially in a CCR2-dependent manner. *The Journal of Immunology,* **2009, 183: 3053–3063.**

The thymus is vital for development of T cells. T progenitor cells in the thymus are subjected to positive and negative selection, and survivors become self-MHC-restricted and self-tolerant mature naive T cells. Negative selection induces clonal deletion of potentially pathogenic autoreactive T cells and consequently decreases the risk of the development of autoimmune disorders (1). Thus, negative selection has a major role in central tolerance. Medullary thymic epithelial cells (mTECs)[2] are major inducers of negative selection. mTECs express the *autoimmune regulator (AIRE)* gene, which induces the ectopic expression of a milieu of peripheral tissue-specific Ags in the thymus resulting in the clonal deletion of autoreactive T progenitors with specificity for these Ags (2–4). Another type of thymic APCs, in particularly dendritic cells (DCs), have also been shown to contribute to negative selection (5–7). However, the detailed molecular and cellular mechanisms by which thymic DCs mediate negative selection remain largely unknown.

Thymic DCs are heterogeneous, similar to DCs in peripheral lymphoid organs such as lymph nodes and spleen. In humans and mice, thymic DCs are classified into two distinct subsets, CD11c$^+$B220$^+$ plasmacytoid DCs (pDCs) and CD11c$^+$B220$^-$ conventional DCs (cDCs). cDCs are further divided into CD11c$^+$CD11b$^-$CD8α^+Sirpα^- and CD11c$^+$CD11b$^+$CD8α^-Sirpα^+ subsets (8, 9). CD8α^+Sirpα^- cDCs, the most abundant subset among these three thymic DC subsets, are clustered in the medulla (10, 11). These CD8α^+Sirpα^- cDCs also express AIRE and can present endogenous self-Ags. In addition, they can cross-present tissue-specific Ags derived from the mTECs for negative selection (12, 13). In contrast, the intrathymic location and functions of another minor cDC, CD11c$^+$CD11b$^+$CD8α^-Sirpα^+, subset remain unclear, although this subset is presumed to migrate from the bloodstream (8). Proietto et al. (14) demonstrated that Sirpα^+ cDCs can induce thymocytes to efficiently differentiate into regulatory T cells in vitro. However, the roles of Sirpα^+ cDCs in central tolerance and regulatory T cell generation in vivo and the nature of the target autoantigens of central tolerance remain elusive.

Chemokines and their receptors have essential roles in controlling the homeostatic homing of immune cells including DCs and T cells (15–17). We examined the composition of thymic DC subsets in mice deficient in CCR1, CCR2, CCR5, or CX3CR1, the chemokine receptors which are expressed by DCs (18, 19). We observed that Sirpα^+ cDCs, but not Sirpα^- cDCs or pDCs, were selectively decreased in the thymus of CCR2-deficient mice, but not in the other chemokine receptor gene-deficient mice. Interestingly, CCR2-deficient mice exhibited a modest impairment in intrathymic negative selection against i.v. injected Ags. Concomitantly, CCR2 deficiency allowed releasing more autoreactive T cells against serum Ags into periphery. These Sirpα^+ cDCs migrated from bone marrow to thymus by the way of the peripheral blood and showed a unique intrathymic localization confined to perivascular and cortical areas. Moreover, Sirpα^+ cDCs had a greater capacity to uptake blood-borne Ags than Sirpα^- cDCs, along with their unique intrathymic localization. Thus, our present study suggests that thymic Sirpα^+ cDCs may function as a specialized APC for the development of central tolerance to blood-borne Ags.

*Division of Molecular Bioregulation, Cancer Research Institute and †Department of Disease Control and Homeostasis, Graduate School of Medical Science, Kanazawa University, Kanazawa, Ishikawa, Japan

Received for publication February 13, 2009. Accepted for publication June 8, 2009.

The costs of publication of this article were defrayed in part by the payment of page charges. This article must therefore be hereby marked *advertisement* in accordance with 18 U.S.C. Section 1734 solely to indicate this fact.

[1] Address correspondence and reprint requests to Dr. Naofumi Mukaida, Division of Molecular Bioregulation, Cancer Research Institute, Kanazawa University, 13-1 Takara-machi, Kanazawa 920-0934, Japan. E-mail address: naofumim@kenroku.kanazawa-u.ac.jp

[2] Abbreviations used in this paper: mTEC, medullary thymic epithelial cell; DC, dendritic cell; Sirpα, signal regulatory protein α; pDC, plasmacytoid DC; cDC, conventional DC; WT, wild type; Col IV, type IV collagen; FCM, flow cytometry; CMFDA, 5-chloromethylfluorescien diacetate; Cyt D, cytochalasin D; FSC, forward scatter; SSC, side scatter; DP, double positive.

www.jimmunol.org/cgi/doi/10.4049/jimmunol.0900438

Materials and Methods

Mice

Specific pathogen-free 6- to 7-wk-old male BALB/c mice were purchased from Charles River Japan and designated as wild-type (WT) mice. CCR1$^{-/-}$ and CX3CR1$^{-/-}$ mice were provided by Dr. P. M. Murphy (National Institute of Allergy and Infectious Diseases, National Institutes of Health, Bethesda, MD) (20, 21). CCR2$^{-/-}$ (22) and CCR5$^{-/-}$ mice (23) were provided by Dr. W. Kuziel (University of Texas San Antonio, San Antonio, TX) and Dr. Kouji Matsushima (University of Tokyo, Tokyo, Japan), respectively. All chemokine receptor-deficient mice were backcrossed to BALB/c mice for 8–10 generations. DO11.10 mice expressing a transgenic TCR that recognizes the $OVA_{323–339}$ peptide in the context of I-A^d were maintained as heterozygotes. DO11.10 mice were backcrossed to CCR2$^{-/-}$ mice to generate DO11.10/CCR2$^{-/-}$ mice. Genotyping for the *CCR2* gene was done by direct PCR from whole blood samples using an Ampdirect Plus kit (Shimadzu) and the specific primers (sense, 5′-CACGAAGTATCCAAGAGCTTG-3′ and antisense, 5′-CCCAAGTGAC TACACTTGTTA-3′). The mouse experiments were performed under specific pathogen-free conditions in accordance with the Guidelines for the Care and Use of Laboratory Animals of Kanazawa University.

Antibodies

Rat anti-mouse mAbs used were anti-CD3ε (145-2C11; Miltenyi Biotec), anti-CD4 (RM4-5; BD Pharmingen), anti-CD8 (53-6.7; BD Pharmingen), anti-CD25 (PC61; BD Pharmingen), anti-CD45R/B220 (RA3-6B2; BD Pharmingen), anti-CD172a/Sirpα (P84; BD Pharmingen), anti-DO11.10 clonotypic TCR (KJ1-26; BD Pharmingen), anti-F4/80 (A3-1; Serotec), and anti-Ly51 (6C3; BioLegend). Hamster anti-mouse CD11c (HL-3) and mouse anti-mouse I-A^d (AMS-32.1) mAbs were purchased from BD Pharmingen. Rabbit anti-mouse CCR2 mAb and anti-mouse type IV collagen (Col IV) polyclonal Ab were purchased from Epitomics and LSL, respectively. Goat anti-mouse MCP-2 polyclonal Ab was purchased from Santa Cruz Biotechnology. Isotype-matched control IgGs for each rat and hamster mAbs were purchased from BD Pharmingen. Mouse, rabbit, and goat IgG (Sigma-Aldrich) served as controls.

Cell preparation

Thymus was digested in 0.6 mg/ml collagenase type IV (Sigma-Aldrich) and 25 Kunitz units/ml DNase I (Sigma-Aldrich) in RPMI 1640 (Sigma-Aldrich) at 37°C for 20 min. The low-density cells were further isolated from the resultant single-cell suspensions using Histopaque-1077 reagent (Sigma-Aldrich). PBMCs were isolated from whole blood using Histopaque-1083 reagent (Sigma-Aldrich). Bone marrow cells were washed out with cold RPMI 1640 medium from the femoral and tibial bones.

Flow cytometry (FCM)

The low-density cells from thymus, PBMCs, and bone marrow cells were stained with various combinations of fluorescent dye-conjugated or nonconjugated specific Abs in PBS supplemented with 2 mM EDTA and 3% FBS. For nonconjugated Abs, fluorescent-conjugated secondary Abs were used. After washing in PBS, expression of cell surface molecular markers was analyzed using a FACSCalibur (BD Biosciences) with CellQuest Pro software (BD Biosciences).

Histology and fluorescent immunohistochemistry

Thymic tissues were frozen in OCT compound (Sakura) and 6-μm-thick cryostat sections were stained with H&E. For immunofluorescence analysis, 6-μm-thick cryostat sections were fixed with cold acetone for 3 min and incubated with Protein Block Reagent (DakoCytomation) to block nonspecific binding. Then fluorescent immunostaining was done by the standard method (for details, see the figure legends). After washing with 0.05% Tween 20-PBS, slides were mounted in fluorescent mounting medium (DakoCytomation). Immunofluorescence was detected in a setting that excluded the nonspecific signal of the isotype control using a fluorescence microscope (BX50; Olympus) or confocal laser-scanning microscope (LSM510; Zeiss). DP Controller software (Olympus) and Zen 2007 software (Zeiss) were used for image processing.

RT-PCR

Total RNAs were extracted from tissues using a RNeasy Mini Kit (Qiagen) and then reverse-transcribed using SuperScript III First-Strand Synthesis System (Invitrogen). PCR was done using the cDNAs, 2.5 mM dNTP mix (Takara), TaqDNA polymerase (Takara), and the specific primer sets for the *GAPDH* gene (sense, 5′-CAC TGA GCA TCT CCC TCA CA-3′ and antisense, 5′-TGG GTG CAG CGA ACT TTA TT-3′), *CD45* gene (sense, 5′-AAG ACA GAG TGC AAA GGA GAC-3′ and antisense, 5′-TGT AGG TGT TTG CCC TGT GAC AAA GAC-3′), *keratin 8* gene (sense, 5′-ACG GTG AAC CAG AGC CTG T-3′ and antisense, 5′-CTC CAC TTG GTC TCC AGC AT-3′), *MCP-1* gene (sense, 5′-CCC ACT CAC CTG CTG CTA CT-3′ and antisense, 5′-TCT GGA CCC ATT CCT TCT TG-3′), *MCP-2* gene (sense, 5′-CAG TCA CCT GCT GCT TTC AT-3′ and antisense, 5′-ATA CCC TGC TTG GTC TGG AA-3′), and *MCP-3* gene (sense, 5′-AAA CAA AAG ATC CCC AAG AGG-3′ and antisense, 5′-CAC AGA CTT CCA TGC CCT TC-3′) for 30 cycles of 95°C for 30 s, 55°C for 30 s, and 72°C for 30 s.

Effects of a peptide Ag on DO11.10 clonotypic thymocytes

DO11.10-transgenic mice with or without *CCR2* gene deficiency were administered 200 μg of $OVA_{323–339}$ peptide (ABGENT) in PBS through the tail vein. To induce thymocyte deletion independently of Ag presentation, mice were injected i.p. with 50 μg of anti-CD3ε mAb (24). Two days after injection, thymocytes were collected and stained with the following combinations of Abs: anti-CD4, anti-CD8, and anti-DO11.10 or anti-CD4, anti-CD25, and anti-DO11.10 Abs. To detect apoptotic cells, thymocytes were stained using an Annexin V-FITC Apoptosis Detection Kit (Merck). After being stained, the cells were analyzed by FCM.

Trafficking of bone marrow-derived immature DCs injected into bone marrow

Bone marrow cells were cultured in RPMI 1640 medium supplemented with 10% FBS and mouse GM-CSF (R&D Systems) at a concentration of 20 ng/ml. An equal volume of culture medium of the same content was added at 4 days, and one-half of the medium was replaced with fresh culture medium at 7 days after the plating. Most bone marrow cells were differentiated into immature DCs as judged by morphological appearances at 10 days after the initiation of the culture. The resultant immature DCs were stained with 1 μM 5-chloromethylfluorescein diacetate (CMFDA; Invitrogen) dye and 1 million cells were injected into the tibial bone marrow cavity of each mouse. After the injection, low-density cells were obtained from thymus, lymph nodes, or PBMCs to determine the presence of CMFDA-stained DCs by using FCM.

Localization of the i.v. injected Ags

Alexa Fluor 488-conjugated OVA protein (OVA_{488}), Alexa Fluor 647-conjugated OVA protein (OVA_{647}) (Invitrogen), or mouse serum IgG (Sigma-Aldrich), which was conjugated with Alexa Fluor 647, using an Alexa Fluor 647 protein labeling kit (Invitrogen), was injected into the tail vein of mice. Thymic low-density cells and PBMCs were isolated at the indicated time points after OVA protein injection and were stained with anti-CD11c and anti-Sirpα Abs. Then the cells were analyzed by FCM. For the localization of the Ag uptake, cryostat sections of frozen thymic tissues were obtained from mice injected with OVA protein and were stained with anti-Sirpα, anti-CD11c, anti-I-A^d, anti-Ly51, or anti-Col IV Abs and were then observed by fluorescence microscope.

In vitro endocytosis assay

Low-density cells were isolated from the thymus and were incubated with 10 μg/ml OVA_{647} in RPMI 1640 at 37°C for 20 min. As a negative control, incubation was conducted on ice. Endocytosis by each thymic DC subset was analyzed by FCM after being stained with anti-CD11c and anti-Sirpα Abs. In some experiments, low-density cells were preincubated with 10 μM cytochalasin D (Cyt D; Sigma-Aldrich), an actin inhibitor (25), 100 mM ammonium chloride (NH_4Cl) (Wako), an inhibitor of the clathrin-dependent pathway (26), or 0.5 mg/ml mannan (Sigma-Aldrich) at 37°C for 15 min before incubation with OVA_{647} at 37°C for 20 min in the presence of fresh inhibitors.

Adoptive transfer of bone marrow cells

Bone marrow cells were obtained from WT or CCR2$^{-/-}$ mice and were stained with 2 μM CMFDA dye. Twenty million cells were injected into the tail vein of CCR2$^{-/-}$ mice. OVA_{647} was injected into the tail vein at 2 days after injection. Thymic low-density cells were isolated at 1 h after OVA protein injection, and the presence of donor-derived Sirpα^+ cDCs and their capability of Ag uptake were analyzed by FCM.

In vivo cell proliferation assay

Spleen mononuclear cells were isolated from WT or CCR2$^{-/-}$ mice and were labeled with 25 μM CFSE using a CellTrace CFSE Cell Proliferation Kit (Invitrogen). Ten million prelabeled cells were injected into the tail vein of WT mice. One day after injection, mice were immunized with total

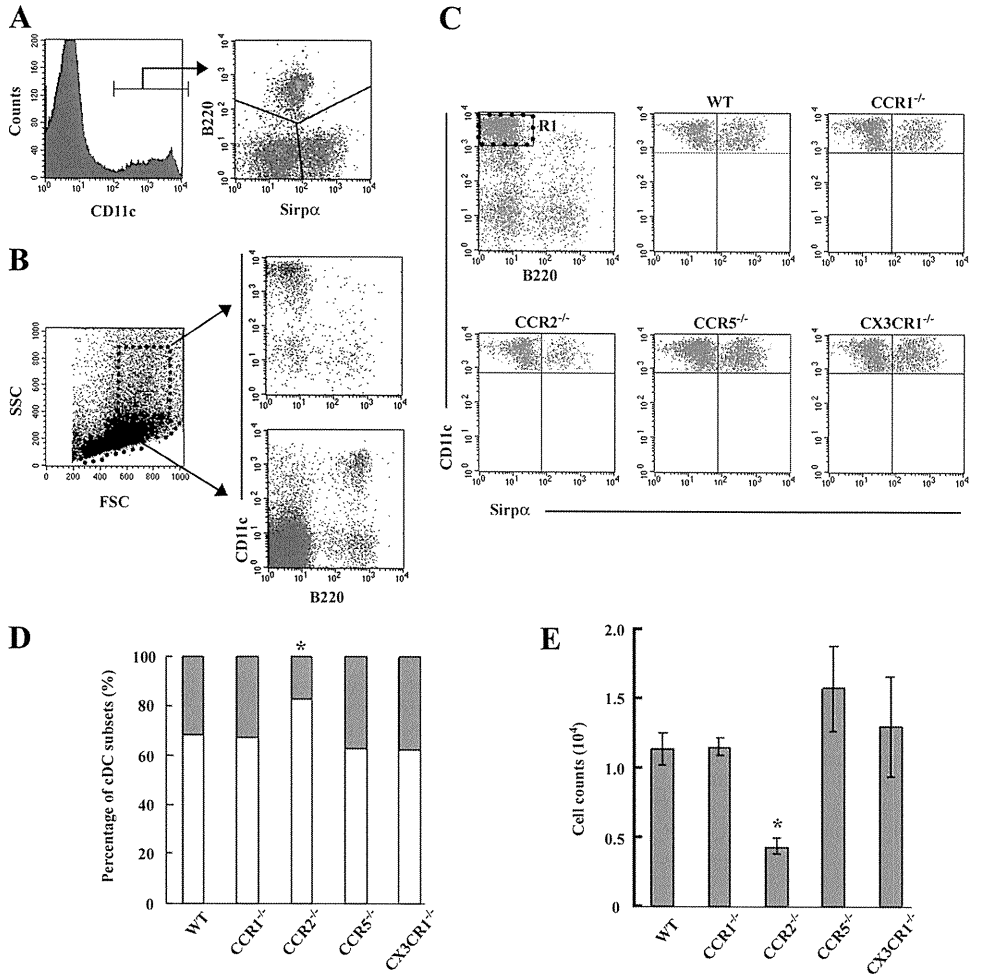

FIGURE 1. Effects of chemokine receptor deficiency on mouse thymic DC subsets. *A*, Low-density cells were isolated from WT mouse thymus and were stained with PE-conjugated anti-CD11c, allophycocyanin-conjugated anti-B220, and nonconjugated anti-Sirpα mAbs, followed by staining with FITC-conjugated mouse anti-rat IgG1. The $CD11c^+$ DC populations were gated to analyze the expression of Sirpα and B220. *B*, Thymic low-density cells were divided into two groups based on their FSC and SSC patterns, which are indicated by elliptic and square gates. Then DC subsets in each region were analyzed. *C*, Low-density cells were isolated from WT, $CCR1^{-/-}$, $CCR2^{-/-}$, $CCR5^{-/-}$, and $CX3CR1^{-/-}$ mice. The $Sirp\alpha^-$ and $Sirp\alpha^+$ subsets in FSC^{high} $SSC^{high}CD11c^{high}B220^-$ cDC populations gated with region 1 (R1) were compared among these mice. *D*, The ratio of two DC subsets (blank portion, $Sirp\alpha^-$ subset; gray portion, $Sirp\alpha^+$ subset) present in thymic cDC population was determined. Data represent the mean of three independent experiments. *E*, The numbers of $Sirp\alpha^+$ DCs in the thymus. Data represent mean ± SD from three independent experiments. *, $p < 0.01$.

mouse serum protein emulsified in CFA. PBS in CFA was immunized as a control. Two days after immunization, lymphocytes were harvested from draining and nondraining lymph nodes and stained with anti-CD4 mAb. The percentage of CFSE-diluted divided cells was analyzed by FCM.

Statistical analysis

Data are represented as mean ± SD. Statistical significance was determined by one-way ANOVA followed by the Tukey-Kramer test. A value of $p < 0.05$ was considered statistically significant.

Results

Selective reduction of thymic $Sirp\alpha^+$ cDCs in $CCR2^{-/-}$ mice

Consistent with a previous report (8), three distinct populations of thymic $CD11c^+$ DCs have been identified: $B220^+$ pDC, $B220^-$ $Sirp\alpha^-$ cDC, and $B220^-Sirp\alpha^+$ cDC subsets (Fig. 1*A*). cDC and pDC subsets were present mainly in the forward scatter (FSC^{high}), side scatter SSC^{high}, and SSC^{low} areas upon FCM, respectively (Fig. 1*B*). The pivotal role of chemokines in the trafficking of DCs prompted us to examine thymic DC subsets in mice deficient in chemokine receptor genes. $Sirp\alpha^+$ DCs were markedly decreased in $CCR2^{-/-}$ mice, compared with WT mice, both in the relative (Fig. 1, *C* and *D*) and absolute number (Fig. 1*E*), whereas $Sirp\alpha^-$ DC (Fig. 1*C*) and $B220^+$ pDC numbers (data not shown) were not changed in $CCR2^{-/-}$ mice. In contrast, no significant changes were observed on thymic cDC and pDC subsets in mice deficient in other chemokine receptors including CCR1, CCR5, and CX3CR1. Moreover, we did not observe any differences in thymic $B220^+$ B cell and $F4/80^+$ macrophage numbers between WT and $CCR2^{-/-}$ mice (data not shown). Microscopic studies of the thymus failed to reveal any morphological differences between WT and $CCR2^{-/-}$ mice in terms of the total cellularity, the distribution of thymocytes in each developmental stage, and the localization of $Ly51^+$ cortical thymic epithelial cells and $I\text{-}A^{d\ high}$ mTEC (supplemental Fig. S1[3]). Thus, $CCR2^{-/-}$ mice exhibit a selective decrease in the $Sirp\alpha^+$ DC subset in thymus.

Attenuation of $OVA_{323-339}$ peptide-induced clonal deletion by CCR2 gene ablation

$Sirp\alpha^+$ DCs are presumed to have the capacity to carry peripheral tissue Ags into the thymus (14). We next investigated the roles of $Sirp\alpha^+$ DCs in thymus on taking in an i.v. administered Ag. PBS injection did not cause any changes in each developmental stage of thymocytes in DO11.10 and DO11.10/$CCR2^{-/-}$ mice (data not shown). On the contrary, i.v. administration of $OVA_{323-339}$ peptide markedly reduced the proportion and absolute number of clonotypic CD4/CD8 double-positive (DP) thymocytes in DO11.10 mice. *CCR2* gene ablation modestly attenuated this reduction (Fig. 2, *A–C*). OVA peptide injection consistently increased the proportion of annexin V^+ apoptotic cells in DO11.10 mouse thymus compared with that in DO11.10/$CCR2^{-/-}$ mice (Fig. 2*D*). In contrast, OVA peptide induced a modest increase in the number of $DO11.10^+CD25^+CD4^+$ regulatory T cell phenotype to similar extents in both DO11.10 and DO11.10/$CCR2^{-/-}$ thymus (Fig. 2*E*). Thus, decreased thymic $Sirp\alpha^+$ DCs in $CCR2^{-/-}$ mice may be associated with a moderately impaired thymic negative selection. Moreover, following i.p. injection with anti-CD3 Ab (24), thymocytes were deleted to similar extents in DO11.10 and DO11.10/$CCR2^{-/-}$ mice

[3] The online version of this article contains supplemental material.

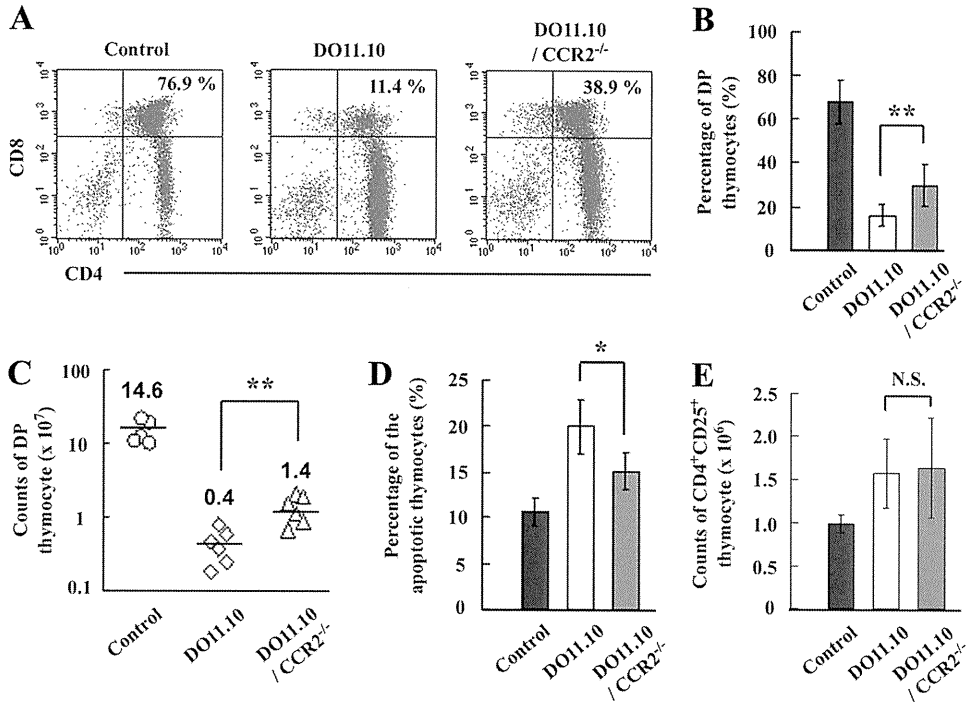

FIGURE 2. Induction of clonal deletion of DO11.10 clonotypic thymocytes. To induce the clonal deletion, 200 μg of $OVA_{323-339}$ peptide in PBS was injected into the tail vein of DO11.10-transgenic or DO11.10/$CCR2^{-/-}$ mice. PBS was injected as a control. DO11.10-transgenic TCR-expressing thymocytes were identified as KJ1-26-positive cells. *A*, Each developmental stage of thymocytes after $OVA_{323-339}$ peptide injection. Percentage of DP stage is shown in each panel. *B*, Percentage of DP stage of development; *C*, the number of DP thymocytes; *D*, percentage of the apoptotic thymocytes; and *E*, the number of $CD4^+$ $CD25^+$ thymocytes were determined on DO11.10 and DO11.10/$CCR2^{-/-}$ mice. Representative results from at least four independent experiments are shown in *A* while the mean ± SD was calculated on at least four independent experiments and are shown in *B–E*. *, $p < 0.05$ and **, $p < 0.01$. N.S., No significant difference.

(supplemental Fig. S2), indicating the absence of intrinsic defects of thymocytes in the absence of CCR2. These results collectively suggest that thymic Sirpα+ DCs can contribute to intrathymic negative selection of a bloodstream-derived Ag without inducing regulatory T cells.

Thymic Sirpα+ DCs can efficiently capture peripheral Ag from bloodstream

To elucidate the functions of thymic Sirpα+ DCs more in detail, we determined their intrathymic localization. In thymi of WT mice, Sirpα was mainly detected on $CD11c^+$ DCs scattered in the thymic cortex (Fig. 3, *A* and *B*), but not on $CD11c^+$ DCs clustered in medulla, the predominating site of thymic $CD8\alpha^+Sirp\alpha^-$ DCs. Moreover, most Sirpα+ DCs were localized in close proximity to small vessels with single Col IV^+ basement membrane or inside perivascular regions (PVRs) separated by two Col IV^+ basement membranes in the cortex (Fig. 3*C*). The thymic DC population includes APCs crucially involved in the central tolerance system involving bloodstream C5 Ag (27). Furthermore, Sirpα+ DCs are selectively localized in PVRs or in close proximity to small vessels, both essential components of the blood-thymus barrier (28). Hence, we hypothesized that this DC subset might be involved in Ag uptake from the bloodstream. To address this possibility, we treated WT mice i.v. with OVA_{647} and examined its uptake by thymic DCs. Intrathymic Sirpα+ DCs, but not Sirpα− DCs, took up OVA protein in a dose-dependent manner (Fig. 4*A*), maintaining a stable level from 1 to 4 h after the injection and decreasing thereafter (Fig. 4*B*). Recently, it was reported that bloodstream DCs could efficiently capture and transport particulate bacteria into the spleen when particulate bacteria were i.v. injected (29). Indeed, bloodstream $CD11c^+$ cells rapidly disappeared from the peripheral blood after capturing OVA protein (Fig. 4*C*). By contrast, the uptake by intrathymic Sirpα+ DCs reached a peak level at 15 min, decreasing to the stable level thereafter. Thus, there may be a remote possibility that circulating DCs migrated into the thymus after capturing OVA protein inside the bloodstream. Furthermore, in addition to an exogenous protein, intrathymic Sirpα+ DCs also captured an endogenous serum protein, mouse IgG, which was conjugated with Alexa Fluor 647, when it was administered i.v. (supplemental Fig. S3). Thus, Sirpα+ DCs can effectively capture peripheral Ags from the bloodstream across the blood-thymus barrier. This notion was further supported by the observation that Sirpα+ DCs engulfed OVA protein with a higher efficiency than Sirpα− DCs when cultured in vitro with OVA_{647} (Fig. 4, *D* and *E*). Mannan from *Saccharomyces cerevisiae*, but not NH_4Cl or Cyt D from *Zygosporium mansonii*, markedly inhibited endocytosis of OVA protein by Sirpα− DCs (Fig. 4*F*, *upper panel*). On the contrary, uptake of OVA protein by Sirpα+ DCs was markedly attenuated by NH_4Cl and Cyt D, but not mannan (Fig. 4*F*, *lower panel*). These observations suggest that thymic Sirpα+ DCs can endocytose soluble Ags more efficiently than Sirpα− DCs, in a clathrin-dependent, but not mannose receptor-dependent manner.

Thymic Sirpα+ DCs capture peripheral Ag inside PVRs or nearby small vessels, and then migrate into the cortical parenchyma

We examined sequentially intrathymic localization of OVA-derived signals after i.v. injection of OVA_{488}. By 0.5 h, OVA_{488}-derived signals were detected in Sirpα+ cells (Fig. 5*A*), $CD11c^+$ DCs (Fig. 5*B*) and inside PVRs or in close proximity to small vessels (Fig. 5*C*). Although some signals remained nearby in small vessels, signals inside PVRs were obviously decreased at 6 h (Fig. 5*D*), as judged by the Col IV immunostaining pattern. At 18 h after the injection, OVA_{488}-derived signals were mainly scattered in the $Ly51^+$ cortical area but not in the $I\text{-}A^{d\ high}$ medullary area (Fig. 5*E*). Because OVA_{488}-derived signals were constantly detected in Sirpα+ DCs at every time point (data not shown), these observations suggest that Sirpα+ DCs initially capture bloodstream OVA protein inside PVRs or in nearby small vessels and then migrate into the cortical parenchyma. To examine the process of migration more in detail, OVA_{647} (blue) and OVA_{488} (green) were i.v. injected sequentially with an interval of either 6 or 18 h as shown in Fig. 5*F*. When OVA_{488} was injected 6 h after OVA_{647}, double-positive $CD11c^{high}$ DCs were evidently detected (8.1%), while single-positive cells were sparse (Fig. 5*F*, *left upper panel*). Even at 18 h after the injection, double-positive $CD11c^{high}$ DCs were still

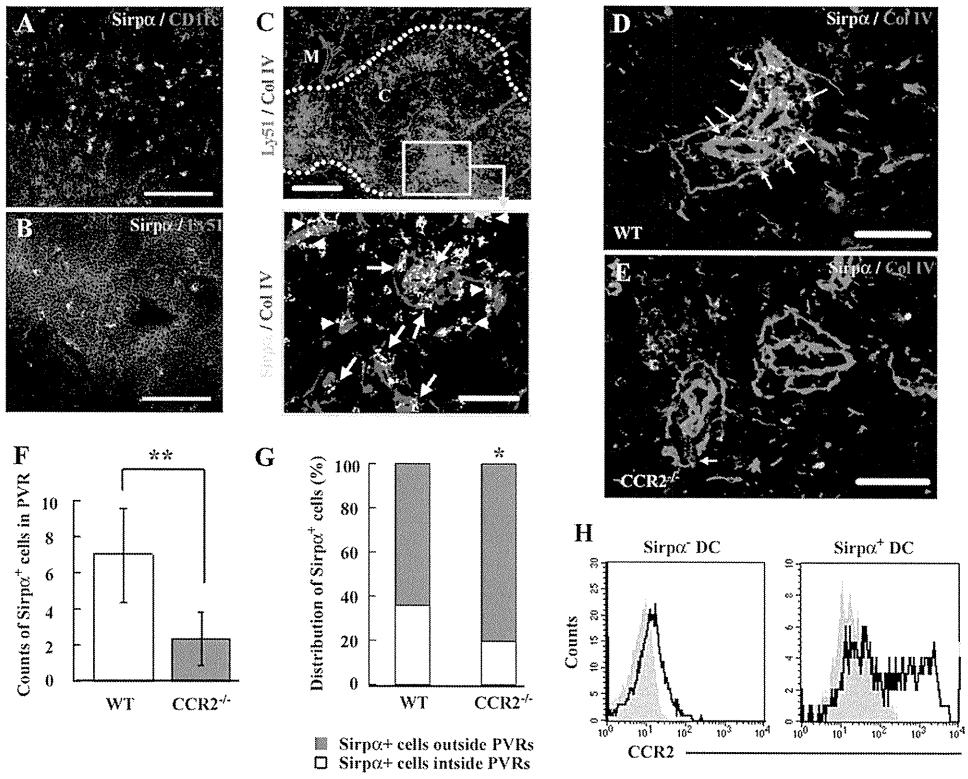

FIGURE 3. Localization of thymic Sirpα^+ DCs. Double-color fluorescence immunostaining for Sirpα (green) and CD11c (red; *A*), Ly51 (red; *B*), or Col IV (red; *D* and *E*). *C*, Triple-color fluorescent immunostaining for Sirpα (green), Ly51 (red), and Col IV (blue). Low magnification image for Ly51 and Col IV is shown in the *upper panel*. A green square in the *upper panel* is observed at a higher magnification for Col IV and Sirpα expression and is shown in the *lower panel*. Dashed lines indicate the boundary between cortex (C) and medulla (M). Arrowheads in *C* and arrows in *C–E* indicate Sirpα^+ cells interacting with small vessels and inside the PVRs, respectively. *A–D*, WT thymus. *E*, CCR2$^{-/-}$ thymus. Representative results from at least two independent experiments are shown here. Scale bars: *A* and *B*, 100 μm; *upper panel* of *C*, 200 μm; *lower panel* of *C–E*, 50 μm. *F* and *G*, At least five photographs in the central regions of the PVRs were taken at $\times$200 magnification in each tissue sample. The numbers of Sirpα^+ cells inside the PVRs were determined and data represent mean $\pm$ SD of three independent experiments. **, $p < 0.01$. *F*, The proportion of Sirpα^+ cells inside the PVRs to outside was calculated and data represent the mean of three independent experiments. *, $p < 0.05$ (*G*). *H*, CCR2 expression on CD11c^{high}Sirpα^- or Sirpα^+ cDCs. Gray-filled and black-open histograms indicate the results from isotype control and specific mAb for CCR2, respectively. Representative results from three independent experiments are shown here.

present (3.2%) with substantial numbers of OVA_{488}-derived signal single-positive (3.9%) or OVA_{647}-derived signal single-positive cells (2.3%; Fig. 5*F*, *left lower panel*). Thus, CD11c^{high} DCs with Sirpα expression can persistently be in close interaction with the bloodstream while they are migrating into cortical parenchyma (Fig. 5*G*).

Depressed migration of Sirpα^+ DCs and their aberrant intrathymic localization in CCR2$^{-/-}$ mice

It is possible that a decreased intrathymic Sirpα^+ DC number may account for the defect in their migration in CCR2$^{-/-}$ mice, because the thymic Sirpα^+ cDC subset is presumed to migrate from the bloodstream (14). Most CD11c$^+$B220$^-$ DCs in peripheral blood and bone marrow expressed abundantly Sirpα (supplemental Fig. S4), similarly as observed on thymic Sirpα^+ DCs, and this population expressed CCR2 (supplemental Fig. S5). CCR2$^{-/-}$ mice exhibited a moderate reduction in CD11c$^+$B220$^-$ DCs in peripheral blood, but not bone marrow (Fig. 6, *A* and *B*). This suggests a possible defect in the migration of CD11c$^+$B220$^-$ DCs from bone marrow in CCR2$^{-/-}$ mice. To test this possibility, bone marrow cells were induced to differentiate to DCs with in vitro GM-CSF stimulation, labeled with CMFDA, and injected into bone marrow of WT mice (Fig. 6*C*, *upper illustration*). Under these conditions, >80% of injected cells expressed CD11c, Sirpα, and CCR2, but not B220 (supplemental Figs. S4 and S5). WT-derived DCs appeared in peripheral blood rapidly within 2 h after the intra-bone marrow injection, whereas CCR2$^{-/-}$ mouse-derived DCs migrated into peripheral blood less efficiently (Fig. 6, *C* and *D*). Interestingly, CD11c$^+$B220$^-$Sirpα^+ DCs appeared in thymus by 6 h after intra-bone marrow injection (Fig. 6*E*). These observations suggest that CCR2-mediated signals were critical of the migration of Sirpα^+ DCs from bone marrow into the thymus. Moreover, Sirpα^+ DCs were markedly decreased in PVRs of CCR2$^{-/-}$ thymus compared with those of WT thymus (WT mice, 7.0 $\pm$ 2.6/site; CCR2$^{-/-}$ mice, 2.3 $\pm$ 1.5/site; Fig. 3, *D–F*). Furthermore, the decrease was more evident in the region inside the PVRs compared with that outside the PVRs (Fig. 3*G*). CCR2 was expressed also by a portion of intrathymic Sirpα^+ DCs, but not Sirpα^- DCs (Fig. 3*H*). Three mouse chemokines, MCP-1, MCP-2, and MCP-3, can bind to CCR2 (30). Among these chemokines, only MCP-2 mRNA was constitutively expressed in thymus, particularly keratin 8-positive thymic stroma, but not CD45-positive thymocytes (Fig. 7, *A* and *B*). Moreover, MCP-2 immunoreactivities were consistently detected inside the PVRs (Fig. 7*C*, *upper panels*) and on Sirpα^+ cells in the PVRs (Fig. 7*C*, *lower panels*). Thus, it is probable that the CCR2-MCP-2 interaction can contribute to intrathymic localization of Sirpα^+ DCs, particularly in the PVRs.

Defective Ag uptake by Sirpα^+ DCs in CCR2$^{-/-}$ mice

Because the PVR was proved to be a main location of the uptake of circulating Ags, we further examined the effects of CCR2

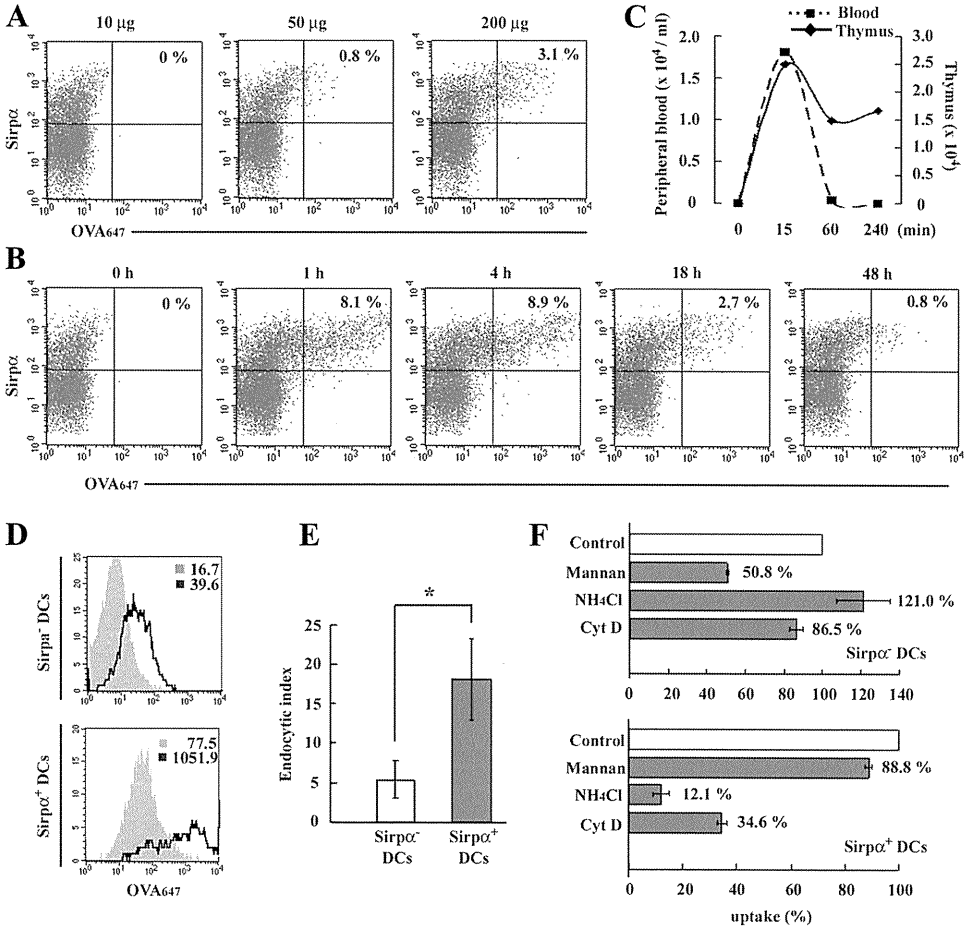

FIGURE 4. Uptake of bloodstream Ag by thymic Sirpα+ DCs. *A*, At 18 h after injection with OVA_{647} at the indicated doses, low-density cells were isolated from WT thymus and were stained with anti-CD11c and anti-Sirpα mAbs. Then the uptake of OVA_{647} in the $CD11c^{high}$ DC population was analyzed. *B*, Uptake of OVA_{647} at the indicated time points. OVA_{647} (200 μg) was injected into the tail vein. Percentage of $Sirp\alpha^+OVA_{647}^+$ region is shown in each panel of *A* and *B*. Representative results from three independent experiments are shown. *C*, Time kinetics of the numbers of DCs capturing OVA protein in the peripheral blood (broken line) and thymus (solid line). *D*, In vitro endocytosis of OVA_{647} by $CD11c^{high}Sirp\alpha^-$ and $CD11c^{high}Sirp\alpha^+$ cDCs are shown in the *upper* and *lower panels*, respectively. Gray-filled and black-open histograms indicate the results obtained when the cells were incubated at 0 and 37°C, respectively. Numbers in each panel indicates mean fluorescence intensity for OVA_{647} captured. Representative results from three independent experiments are shown here. *E*, Endocytic index in $Sirp\alpha^-$ and $Sirp\alpha^+$ cDCs. Endocytic index was calculated as mean fluorescence intensity at 37°C/mean fluorescence intensity at 0°C. Mean ± SD were calculated from three independent experiments and are shown here. *, $p < 0.01$. *F*, The effects of various agents on endocytosis. Uptake in the presence of each inhibitor is shown as the percentage of total uptake in the absence of any inhibitors. Means were calculated from three independent experiments and are shown here.

deficiency on the capability of $Sirp\alpha^+$ DCs to uptake Ags from the bloodstream. Indeed, when OVA_{647} was injected i.v., $CCR2^{-/-}$ mice exhibited a reduced proportion of intrathymic DCs capturing OVA protein compared with WT mice (Fig. 8, *A* and *B*). Moreover, after the OVA_{647} injection, $Sirp\alpha^+$ DCs of WT mice contained a substantial proportion of OVA^{high} cells, which represent the cells with a higher uptake of OVA protein, and this population was markedly reduced in $CCR2^{-/-}$ mice (Fig. 8, *C* and *D*). Moreover, among $Sirp\alpha^+$ DCs, the CCR2-expressing population was a main cell type which captured OVA protein (Fig. 8*E*). CMFDA-labeled WT mouse-derived bone marrow cells appeared in thymus 2 days after the adoptive transfer to CCR2-deficient mice and a substantial proportion of these stained cells expressed CD11c and Sirpα simultaneously (Fig. 8*F*). $Sirp\alpha^+CD11c^+$ DCs appeared in thymus similarly when CMFDA-labeled CCR2-deficient mouse-derived bone marrow cells were adoptively transferred (data not shown). When OVA_{647} was injected i.v. 2 days after the adoptive transfer, WT donor-derived $Sirp\alpha^+CD11c^+$ DCs captured OVA protein more efficiently than CCR2-deficient DCs in the CCR2-deficient thymus (Fig. 8*G*). Thus, CCR2-mediated signals may at least partially regulate the function of $Sirp\alpha^+$ DCs to uptake Ag from the bloodstream (supplemental Fig. S6).

Accumulation of autoreactive T cells against serum Ags in the periphery of $CCR2^{-/-}$ mice

We observed that $CCR2^{-/-}$ mice did not exhibit any signs suggestive of autoimmune disorders until 1 year after the birth (our unpublished data). Hence, we examined whether autoreactive T cells against certain self-Ags in the bloodstream accumulated in the periphery of $CCR2^{-/-}$ mice. We examined the accumulation of autoreactive T cells in the draining lymph nodes in WT mice that received CFSE-labeled WT or $CCR2^{-/-}$ mouse-derived splenocytes and were subsequently immunized with mouse serum emulsified in CFA. Immunization with total serum protein increased the cell division of $CCR2^{-/-}$ mouse-derived $CD4^+$ T cells inside draining lymph nodes (10.6%) to a greater extent than immunization with PBS (4.3%; Fig. 9*A*). Moreover, $CD4^+$ T cell division was significantly increased in the recipients of $CCR2^{-/-}$ mouse-derived splenocytes compared with the recipients of WT mouse-derived splenocytes (Fig. 9*B*). Thus, the lack of CCR2 can

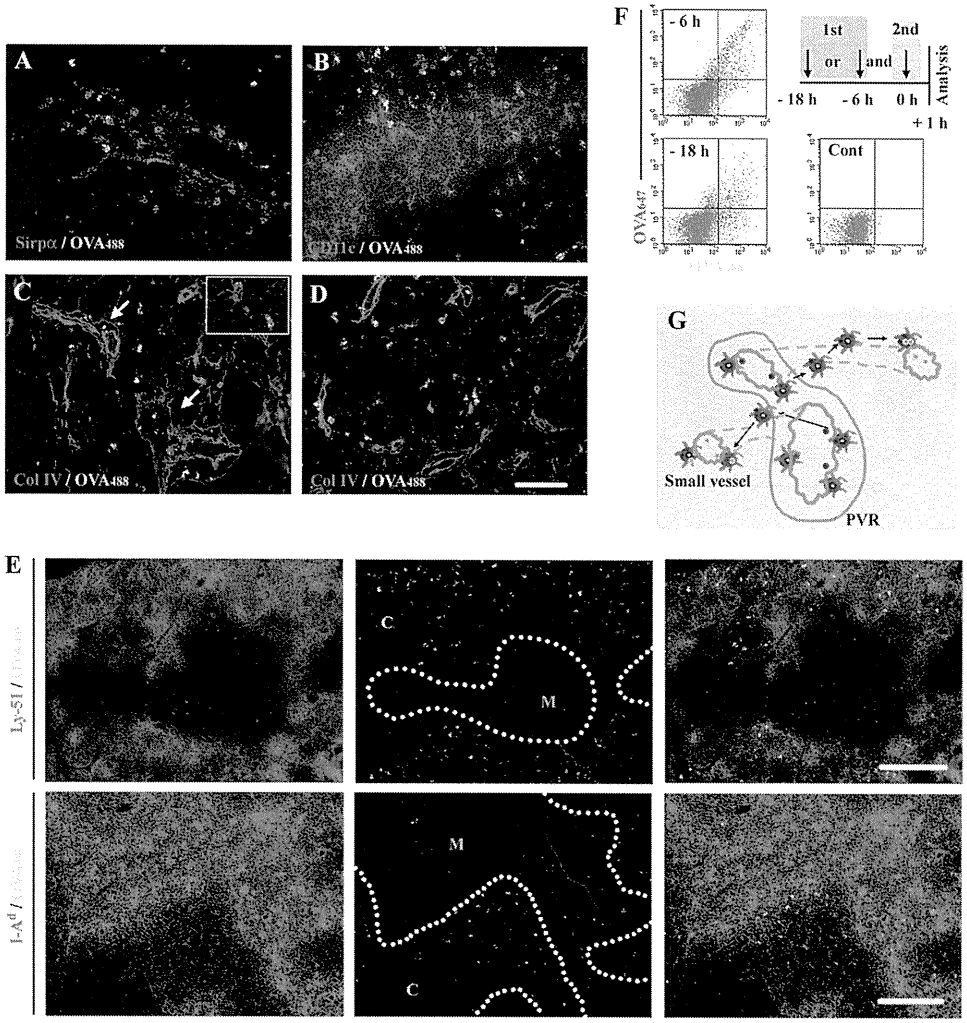

FIGURE 5. Localization of i.v. injected Ag in thymus. *A–C*, Thymic tissues were obtained 0.5 h after injection of OVA_{488} and were stained to obtain a double-color fluorescent image with the combination of OVA_{488} (green) and (*A*) Sirpα (red), (*B*) CD11c (red), or (*C*) Col IV (red). Arrows in *C* indicate the cells with captured OVA_{488} inside the PVRs. The image showing the cells capturing OVA_{488} in close proximity to small vessels is an *inset* in *C*. *D*, A double-color fluorescent image for OVA_{488} (green) and Col IV (red) at 6 h after OVA injection. Scale bars, 100 μm. *E*, A double-color fluorescent image with the combination of OVA_{488} (green) and Ly51 (red) or I-A^d (red) at 18 h after injection is shown in the *upper* and *lower panels*, respectively. The merged images are shown in the *right panels*. Dashed lines indicate the boundary between cortex (C) and medulla (M). Scale bars, 200 μm. *F*, OVA_{647} and OVA_{488} were i.v. injected consequently with an interval of either 6 or 18 h, illustrated in *upper right panel* in *F*. Uptake of OVA protein by $CD11c^{high}$ DC population isolated after double injection with an interval of either 6 or 18 h is shown in the *left upper* and *lower panels*, respectively. Autofluorescence for each parameter in the $CD11c^{high}$ DC population without injection is shown as a control. Representative results from three independent experiments are shown here. *G*, Presumed intrathymic trafficking modes of $Sirp\alpha^+$ DCs, combined with the Ag uptake. Blue and green particles indicate OVA_{647} and OVA_{488}, respectively.

result in enhanced accumulation of autoreactive T cells against serum self-Ags.

Discussion

Mouse thymus $CD11c^+$ cDCs can be classified into two populations, a major $CD8\alpha^+$ and a minor $CD8\alpha^-$ one (31). $CD8\alpha^-$ cDCs can pick up $CD8\alpha\beta$ heterodimer from thymocytes and retain them on the cell surface, thus precluding the use of $CD8\alpha$ as a reliable marker to distinguish these two populations. Wu and Shortman (8) observed that $CD8\alpha^-$ but not $CD8\alpha^+$ cDCs simultaneously express the Sirpα molecule and proposed the use of Sirpα as a marker of this minor cDC population. Concomitantly, it was proposed that the interaction between thymocytes and DCs in thymic cortex can also have profound effects on positive selection (32). Likewise, McCaughtry et al. (33) observed that clonal deletion of autoreactive thymocytes requires the stimuli from rare $CD11c^+$ cortical DCs. Given the unique localization of $Sirp\alpha^+$ DCs confined to the cortex, these observations suggest the potential involvement of $Sirp\alpha^+$ DCs in central tolerance, but their small number hinders the isolation for a detailed analysis of $Sirp\alpha^+$ DC function.

A partial but selective reduction in intrathymic $Sirp\alpha^+$ cDCs in $CCR2^{-/-}$ mice prompted us to investigate the thymic selection process in WT and $CCR2^{-/-}$ mice to elucidate the role of intrathymic $Sirp\alpha^+$ cDCs in the process. When DO11.10 TCR-transgenic mice were administered immunogenic $OVA_{323-339}$ peptide i.v., *CCR2* gene ablation partially attenuated the clonal negative deletion by apoptosis of the $DO11.10^+$ DP thymocyte population. Intraperitoneal injection of anti-CD3 Ab deleted thymocytes to similar extents in WT and $CCR2^{-/-}$ mice, excluding the possibility that CCR2 deficiency impaired the apoptotic response of thymocytes. Negative selection can be exerted by various types of APCs including $Sirp\alpha^-$ cDCs, B cells, macrophages, cortical thymic epithelial cells, and mTEC in addition to $Sirp\alpha^+$ cDCs. We

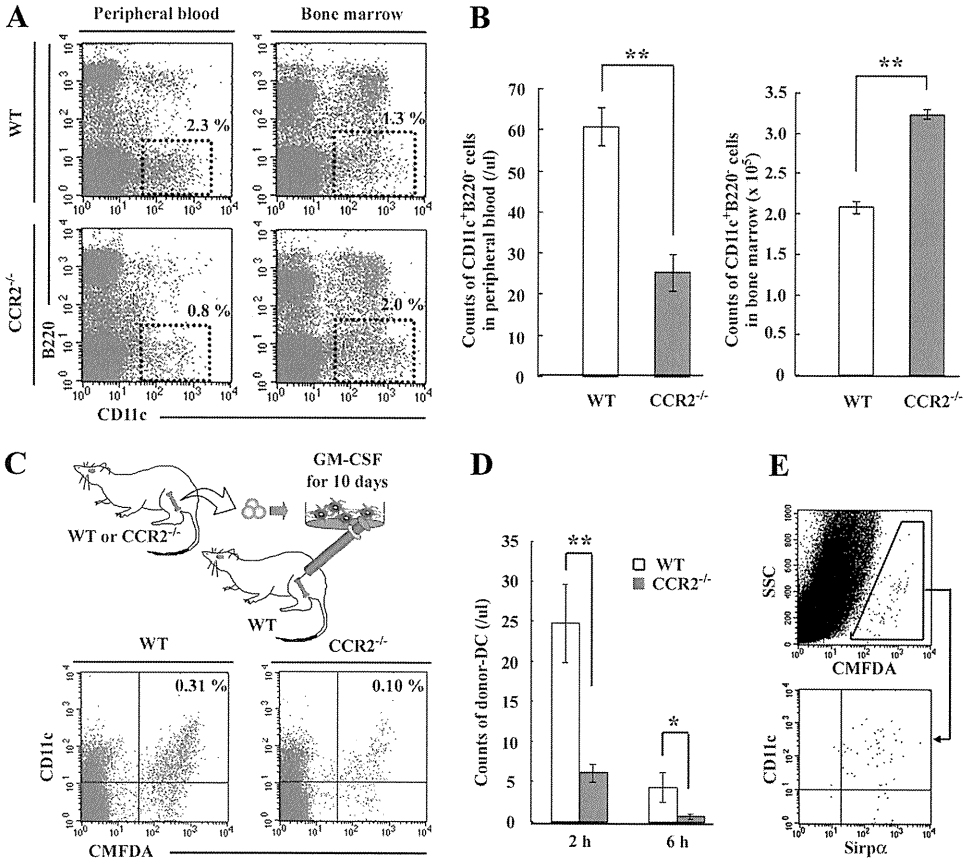

FIGURE 6. Mobilization of Sirpα+ DCs from bone marrow. *A* and *B*, PBMCs and bone marrow cells isolated from femur bone marrow were stained with anti-CD11c and anti-B220 mAbs. Proportion (*A*) and the numbers (*B*) of $CD11c^+B220^-$ cells gated with the dot squares were determined on peripheral blood and bone marrow in $CCR2^{-/-}$ and WT mice. Percentage of gated cells is shown in each panel of *A*. Mean ± SD were calculated from three independent experiments and are shown here. *C*, The image of experimental procedure of "trafficking of bone marrow-derived DCs" was illustrated and is shown in the *upper panel*. PBMCs were isolated from the recipients 2 h after injection and stained with anti-CD11c mAb. Egress of $CCR2^{-/-}$ bone marrow-derived DCs into peripheral blood was compared with WT DCs. Percentage of donor DCs in $CMFDA^+CD11c^+$ region is shown in each panel. *D*, The numbers of donor-derived DCs in peripheral blood were determined 2 and 6 h after injection. Mean ± SD calculated from five independent experiments are shown here. *, $p < 0.05$ and **, $p < 0.01$. *E*, One × 10^7 WT bone marrow cell-derived DCs were injected into both the right and left tibial cavity. Six hours after injection, expression of Sirpα and CD11c on intrathymic migrated $CMFDA^+$ donor cells was analyzed by FCM. Representative results from four independent experiments are shown here.

failed to detect any apparent differences in other APC populations than Sirpα+ cDCs between WT and $CCR2^{-/-}$ mice. Thus, it is unlikely that reduced negative selection in $CCR2^{-/-}$ mice can be ascribed to the changes in these cell populations. Furthermore, accumulating evidence implicates intrathymic $CD4^+CD25^+$ regulatory T cells as an essential cell component in central tolerance.

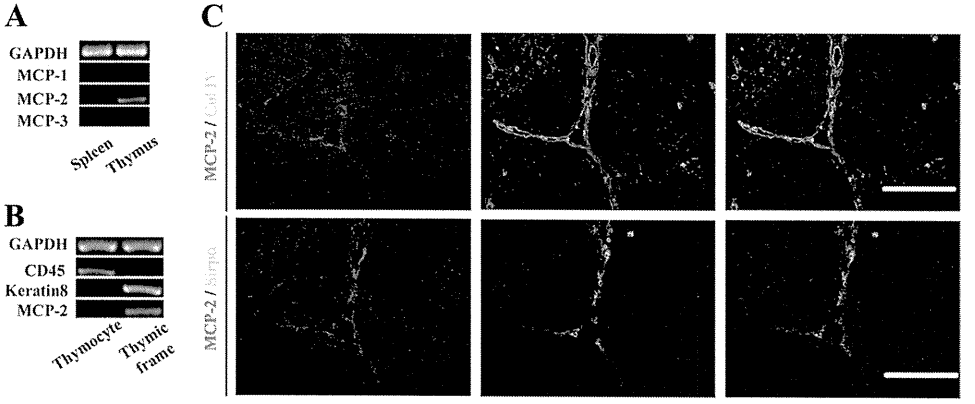

FIGURE 7. Expression of CCR2 ligands in thymus under physiological condition. *A*, Total RNAs were extracted from thymus and spleen of WT mice. Expression of CCR2 ligands, MCP-1, MCP-2, and MCP-3, was determined by RT-PCR. GAPDH served as an internal positive control. *B*, Thymic tissues were mechanically disrupted and fractionated into thymocyte and thymic stromal components. MCP-2 transcripts were determined on these two fractions by RT-PCR. CD45 and keratin 8 served as positive control for the thymocyte and thymic stromal fraction, respectively. *C*, Double-color fluorescent immunostaining for MCP-2 (red) and Col IV (green) or MCP-2 (red) and Sirpα (green) in the thymic tissue sections are shown in the *upper* and *lower panels*, respectively. The merged images are shown in the *right panels*. Representative results from three independent animals are shown here. Scale bars, 100 μm.

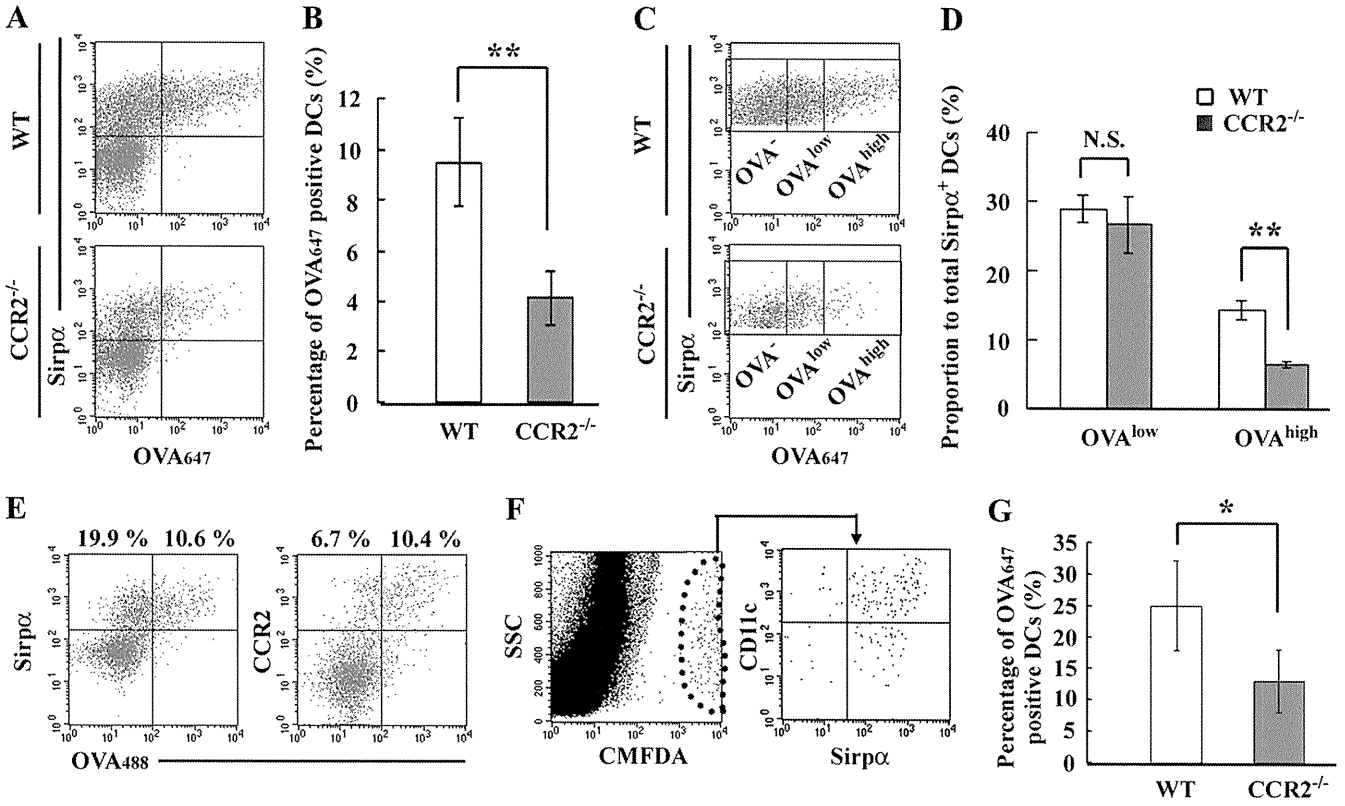

FIGURE 8. Effects of CCR2 deficiency on Ag uptake by thymic Sirpα^+ DCs. *A*, The uptake of OVA_{647} in the CCR2$^{-/-}$ CD11c^{high} DC population at 4 h after i.v. injection was compared with WT-derived cells. *B*, Percentage of DCs capturing OVA_{647} in the CD11c^{high} DC population. Mean ± SD were calculated from five independent experiments and are shown here. **, $p < 0.01$ *C*, Sirpα^+ DCs derived from WT and CCR2$^{-/-}$ thymus were separated into three groups according to the efficiency of OVA_{647} uptake, OVA$^-$; DCs without capturing OVA_{647}, OVA^{low}; DCs capturing OVA_{647} with a low efficiency, and OVA^{high}; and DCs capturing OVA_{647} with a high efficiency. *D*, Percentage of OVA^{low} and OVA^{high} in WT and the CCR2$^{-/-}$ Sirpα^+ DC population. Mean ± SD were calculated from five independent experiments and are shown here. **, $p < 0.01$; N.S., no significant difference. *E*, OVA_{488} was i.v. injected into WT mice. One hour after injection, low-density cells were stained with anti-CD11c and anti-Sirpα or anti-CCR2 mAbs. The uptake of OVA_{488} and expression of Sirpα or CCR2 in the CD11c^{high} DC population are shown. Percentage of Sirpα^+OVA$_{488}^+$ and OVA$_{488}^-$, or CCR2$^+$OVA$_{488}^+$ and OVA$_{488}^-$ regions are shown in the *left* or *right panel*. Representative results from three independent experiments are shown here. *F*, Migration of Sirpα^+ DCs into the thymus at 2 days after i.v. injection of CMFDA-labeled WT bone marrow cells into CCR2$^{-/-}$ mice. Expression of CD11c and Sirpα on CMFDA$^+$ donor-derived cells is shown in the *right panel*. Representative results from three independent experiments are shown here. *G*, OVA_{647} was i.v. injected into CCR2$^{-/-}$ mice at 2 days after injection of bone marrow cells. Percentage of WT and CCR2$^{-/-}$ donor-derived DCs capturing OVA_{647} in the CMFDA$^+$CD11c^{high} region are shown. Mean ± SD were calculated from four independent experiments and are shown here. *, $p < 0.05$.

Indeed, Proietto et al. (14) recently reported the capability of Sirpα^+ cDCs to induce the differentiation of regulatory T cells in vitro. However, OVA peptide injection induced the differentiation of regulatory T cells to similar extents in both DO11.10 and DO11.10/CCR2$^{-/-}$ thymus. Thus, it is probable that CCR2 deficiency reduced modestly intrathymic Sirpα^+ DCs without affecting regulatory cell induction and partially attenuated negative selection in vivo.

It remains elusive on the trafficking modes of Sirpα^+ DCs. In CCR2$^{-/-}$ mice, Sirpα^+ DCs were decreased moderately in peripheral blood and thymus, but were increased in bone marrow. Considering that CCR2 signaling can regulate the mobilization of monocytes from bone marrow to peripheral blood (34, 35), these observations raised the possibility of a defect in the trafficking of Sirpα^+ DCs from bone marrow in CCR2$^{-/-}$ mice. Indeed, WT mouse-derived Sirpα^+ DCs, injected into bone marrow, appeared first in peripheral blood and then the thymus. On the contrary, CCR2$^{-/-}$ mouse-derived Sirpα^+ DCs exhibited impairment in the egress from bone marrow to peripheral blood. These observations suggest that bone marrow-derived Sirpα^+ DCs migrated to peripheral blood in response to CCR2-mediated signals and subsequently traffic to the thymus.

In the thymus, Sirpα^+ DCs were characteristically localized in close proximity to small blood vessels and inside the PVRs, sites which are compartmentalized by a vascular basement membrane and a border membrane separating them from the thymic parenchyma (36). It is of note that Sirpα^+ cells in the PVRs were markedly decreased in CCR2$^{-/-}$ mice to a greater extent than the decrease in total Sirpα^+ cell number. Thus, intrathymic CCR2 signaling can regulate their unique localization. This notion was supported by the observation that MCP-2, a potential ligand for CCR2, was constitutively detected in the PVRs, where Sirpα^+ DCs were present.

PVRs can provide a pathway for hematopoietic progenitor cells and mature T cells to traverse from the bloodstream to the thymic parenchyma (36) and are presumed to constitute the blood-thymus barrier, which can protect the thymic parenchyma from bloodstream-derived macromolecules (28). Thus, the unique localization of Sirpα^+ cDCs in the thymus suggested their potential interactions with bloodstream-derived Ag. This assumption was strengthened by our present observation that intrathymic Sirpα^+ cDCs rapidly and specifically captured OVA protein and serum IgG following i.v. injection. Moreover, injected Ags were initially detected inside PVRs or in nearby small vessels and were subsequently in the cortical parenchyme, and the injected Ag-derived

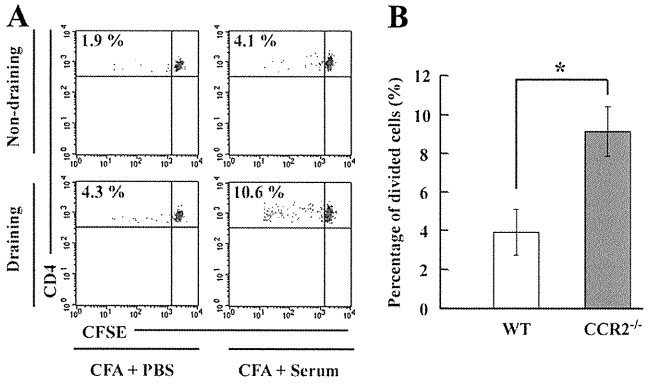

FIGURE 9. Accumulation of autoreactive T cells against serum Ags in the spleen. Spleen mononuclear cells were isolated from WT or $CCR2^{-/-}$ mice and i.v. injected into WT mice after labeling with CFSE. *A*, Recipients of $CCR2^{-/-}$ mouse-derived splenocytes were immunized with total mouse serum or PBS emulsified in CFA at 1 day after injection. Four days after, draining and nondraining lymph nodes were harvested and division of $CFSE^+$ donor-derived $CD4^+$ T cells was analyzed by FCM. Representative results from three independent experiments are shown here. *B*, Percentage of divided $CD4^+$ T cells was determined in the draining lymph nodes of the recipients of either WT-derived or $CCR2^{-/-}$ donor-derived splenocytes when the recipients were immunized with mouse serum emulsified in CFA. Mean ± SD were calculated from three independent experiments and are shown here. *, $p < 0.01$.

signals were consistently colocalized with CD11c and Sirpα. Thus, after $CD11c^+Sirp\alpha^+$ cDCs, located around the PVRs, capture the Ags, they presumably move to cortical parenchyme to educate T cells. Indeed, $CCR2^{-/-}$ thymus-derived $Sirp\alpha^+$ DCs exhibited a reduced capacity to uptake OVA. The lack of CCR2 can hinder the proper intrathymic localization of $Sirp\alpha^+$ DCs and their distinctive function, Ag uptake from bloodstream, thereby reducing Ag presentation in the cortical parenchyma and subsequent negative selection against a blood-borne Ag. This hypothesis is supported by our observation in that $CD4^+$ T cells reactive to certain serum self-Ags accumulated in the periphery of the recipients of $CCR2^{-/-}$ mouse-derived splenocytes to a greater extent than the recipients of WT mouse-derived splenocytes.

DCs can uptake free soluble Ags, in three distinct manners, by clathrin-mediated endocytosis, nonclathrin/caveolae endocytosis, and macropinocytosis (25). Thymic $Sirp\alpha^+$ cDCs could endocytose OVA Ags more efficiently than thymic $Sirp\alpha^-$ cDCs when they were cultured in vitro with OVA Ags. Furthermore, NH_4Cl, an inhibitor of clathrin-mediated endocytosis (26), markedly inhibited OVA endocytosis by $Sirp\alpha^+$ cDCs, but not by $Sirp\alpha^-$ cDCs. On the contrary, OVA protein endocytosis by $Sirp\alpha^-$ DCs was partially inhibited by mannan, whereas mannan had few effects on OVA protein endocytosis by $Sirp\alpha^+$ DCs. These observations suggest that thymic $Sirp\alpha^+$ cDCs characteristically can efficiently endocytose Ags in a manner distinct from thymic $Sirp\alpha^-$ cDCs.

Balazs et al. (29) reported that bloodstream DCs could efficiently capture and transport particulate bacteria into the spleen when particulate bacteria were i.v. injected. We also observed that $CD11c^+$ DCs rapidly disappeared from peripheral blood after uptake of i.v. injected OVA protein. Given the capacity of $CD11c^+$ DCs to move rapidly from blood to thymus, blood $CD11c^+$ DCs may migrate into thymus after capturing the i.v. injected Ag. However, Ag-capturing DCs appeared very rapidly in the thymus, reaching maximal levels before disappearance of Ag-capturing circulating DCs from the peripheral blood. Furthermore, when OVA protein was injected i.v. into mice that contained bloodstream DCs labeled with fluorescent-conjugated latex beads, latex-labeled DCs did not appear in the thymus (our unpublished data). Thus, it is remotely possible that bloodstream DCs captured OVA protein and subsequently migrated into thymus.

In this study, we identified the unique intrathymic localization and functions of thymic $Sirp\alpha^+$ DCs that are involved in negative selection, particularly against blood-borne Ags. Serum protein can also induce negative selection in thymus (27, 37) but the molecular and cellular mechanisms remain to be elucidated. Because $Sirp\alpha^+$ cDCs can uptake serum protein such as IgG, these cells may induce central tolerance to blood-borne-derived Ags, in addition to Ags presented by the well-characterized intrathymic AIRE-mediated pathway.

We have shown that CCR2-mediated signals can regulate various biological aspects of $Sirp\alpha^+$ DCs such as their appropriate intrathymic localization and Ag uptake capacity. It is widely held that CCR2 might be a potential therapeutic target for several autoimmune disorders. However, because CCR2-mediated signals may contribute to thymic negative selection against blood-borne Ags, CCR2 blockade may aggravate autoimmune disorders similar to the observation on the murine collagen-induced arthritis model (38). Moreover, Lauritzsen et al (39) reported that proteins secreted from tumor cells into peripheral blood were transported into the thymus to eventually cause clonal deletion of tumor Ag-specific T cell repertoires. Given the potential capacity of intrathymic $Sirp\alpha^+$ DCs to capture blood-borne Ags, they may have a role in the development of tumor tolerance. Because human thymus contains DCs with similar phenotypes and intrathymic localization as $Sirp\alpha^+$ cDCs (40), a more detailed elucidation of the functions of $Sirp\alpha^+$ cDCs may provide us with useful insights to develop a better therapeutic strategy for cancer and stem cell transplantation as well as autoimmune disorders.

Acknowledgments

We express our gratitude to Drs. Joost J. Oppenheim (National Cancer Institute-Frederick, Frederick, MD) and Nobuyuki Onai (Akita University, Akita, Japan), and Yi Zhang (University of Michigan, Ann Arbor, MI) for critical review of this manuscript. We thank Drs. William Kuziel, Kouji Matsushima, and Philip Murphy for providing us with CCR2-, CCR5-, and CCR1- and CX3CR1-deficient mice, respectively.

Disclosures

The authors have no financial conflict of interest.

References

1. von Boehmer, H., I. Aifantis, F. Gounari, O. Azogui, L. Haughn, I. Apostolou, E. Jaeckel, F. Grassi, and L. Klein. 2003. Thymic selection revisited: how essential is it? *Immunol. Rev.* 191: 62–78.
2. Anderson, M. S., E. S. Venanzi, Z. Chen, S. P. Berzins, C. Benoist, and D. Mathis. 2005. The cellular mechanism of Aire control of T cell tolerance. *Immunity* 23: 227–239.
3. Anderson, M. S., E. S. Venanzi, L. Klein, Z. Chen, S. P. Berzins, S. J. Turley, H. von Boehmer, R. Bronson, A. Dierich, C. Benoist, and D. Mathis. 2002. Projection of an immunological self shadow within the thymus by the aire protein. *Science* 298: 1395–1401.
4. Liston, A., S. Lesage, J. Wilson, L. Peltonen, and C. C. Goodnow. 2003. Aire regulates negative selection of organ-specific T cells. *Nat. Immunol.* 4: 350–354.
5. Anderson, G., K. M. Partington, and E. J. Jenkinson. 1998. Differential effects of peptide diversity and stromal cell type in positive and negative selection in the thymus. *J. Immunol.* 161: 6599–6603.
6. Marrack, P., D. Lo, R. Brinster, R. Palmiter, L. Burkly, R. H. Flavell, and J. Kappler. 1988. The effect of thymus environment on T cell development and tolerance. *Cell* 53: 627–634.
7. Matzinger, P., and S. Guerder. 1989. Does T-cell tolerance require a dedicated antigen-presenting cell? *Nature* 338: 74–76.
8. Wu, L., and K. Shortman. 2005. Heterogeneity of thymic dendritic cells. *Semin. Immunol.* 17: 304–312.
9. Liu, Y. J. 2006. A unified theory of central tolerance in the thymus. *Trends Immunol.* 27: 215–221.
10. Bendriss-Vermare, N., C. Barthelemy, I. Durand, C. Bruand, C. Dezutter-Dambuyant, N. Moulian, S. Berrih-Aknin, C. Caux, G. Trinchieri, and F. Briere. 2001. Human